Spring 2022

Particle swarm optimization for critical experiment design

Cole Michael Kostelac

Department:

PARTICLE SWARM OPTIMIZATION FOR CRITICAL EXPERIMENT DESIGN

by

COLE MICHAEL KOSTELAC

A THESIS

Presented to the Graduate Faculty of the

MISSOURI UNIVERSITY OF SCIENCE AND TECHNOLOGY

In Partial Fulfillment of the Requirements for the Degree

MASTER OF SCIENCE

in

NUCLEAR ENGINEERING

2022

Approved by:

Ayodeji Alajo, Advisor
Syed Alam
Nicholas Thompson

ABSTRACT

Critical experiments are used by nuclear data evaluators and criticality safety engineers to validate nuclear data and computational methods. Many of these experiments are designed to maximize the sensitivity to a certain nuclide-reaction pair in an energy range of interest. Traditionally, a parameter sweep is conducted over a set of experimental variables to find a configuration that is critical and maximally sensitive. As additional variables are added, the total number of configurations increases exponentially and quickly becomes prohibitively computationally expensive to calculate, especially using Monte Carlo methods.

This work presents the development of a particle swarm optimization algorithm to design these experiments in a more computationally efficient manner. The algorithm is then demonstrated by performing a two-dimensional and three-dimensional optimization of a uranium-molybdenum and plutonium-molybdenum critical experiment, respectively.

The two-dimensional and three-dimensional optimizations on average performed 35x and 3277x faster than the parameter sweep method, respectively. This corresponds to a 5.6 day and 2,314 day reduction in computation time.

ACKNOWLEDGMENTS

First, I would like to thank my advisor Dr. Alajo for his guidance and the trust he placed in me when I came to him with this idea. I do not think I would've been able to make this work with anyone else as my advisor. Your first principles approach allowed to me make decisions with confidence.

I would also like to thank all of NEN-2 at Los Alamos, especially my mentors Dr. Nicholas Thompson, Dr. Rene Sanchez and Noah Kleedtke. I feel especially lucky to get to work on the most incredible experiments with the some of the smartest, kindest people I've ever met. I have felt nothing but welcomed. Nick, thank you for answering my endless questions, pushing me to do my best, and encouraging me to continue my education. I could not ask for a better mentor. Rene, thank you for responding to my cold email and taking a chance on me by inviting me to join the group. Noah, thank you for your insight into graduate school and all of the valuable feedback you've given me on papers and presentations, you have been an extremely reliable friend and mentor.

Most importantly, I want to thank my family. Your support and encouragement has taken me to places of awe and wonder in my pursuits, academic and otherwise. Thank you for the telescopes and microscopes, helmets and crampons, and drum sticks and sheet music over the years.

Lastly, I would like to thank my grandparents: Jerome and Sondra Kostelac and Richard and Marceline Desko, to whom this work is dedicated. I have always felt my passion for science was nurtured by you.

TABLE OF CONTENTS

Page

LIST OF ILLUSTRATIONS

LIST OF TABLES

1. INTRODUCTION

1.1. CRITICALITY EXPERIMENTS

Since the dawn of nuclear engineering, criticality experiments have served an integral and irreplaceable role in the advancement of the field. From validating nuclear data and computational modeling methods to establishing subcritical operating limits, these experiments provide data that serves as a reality check for engineers and scientists. Before the development of high performance computing and modern stochastic and deterministic approaches to modeling critical systems, criticality experiments were used to determine the critical masses of fissionable material. Today many critical experiments are used to validate nuclear data and neutron transport methods. By changing the geometry, moderators, or reflectors, an experimenter can create a critical system in different neutron energy regimes.

1.1.1. A Brief History. Criticality experiments in the United States can trace their roots to the Manhattan Project in the 1940's. The first critical mass measurements of highly enriched uranium and plutonium were conducted in Los Alamos, New Mexico [1] [2]. After World War II other critical experiment groups were formed outside of Los Alamos. At their peak in the 1970's there were critical experiment groups at Los Alamos Scientific Laboratory (later Los Alamos National Laboratory), Oak Ridge National Laboratory, Brookhaven National Laboratory, Lawrence Radiation Laboratory (later Lawrence Livermore National Laboratory), Battelle Pacific Northwest Laboratory, and the Rocky Flats Plant [3]. By the year 2000, due to heavier reliance of computational methods and rising security costs, many critical experiments groups in the United States and around the world had ceased operations [3].

In 2004 after over 50 years of operations, the Los Alamos Critical Experiments Facility (LACEF) ceased operations and began to move its fissile material inventory and critical assemblies from Tecnical Area 18 (TA-18) at Los Alamos to the Device Assembly

Facility (DAF) located in the Nevada National Security Site (NNSS), formerly known as the Nevada Test Site [4]. At the time, LACEF was the only facility in the United States capable of providing criticality safety demonstrations, hands-on experience in handling special nuclear material, and characterization of multiplying systems [4]. By 2011 operations resumed at the DAF under a new name: the National Criticality Experiments Research Center (NCERC) [5].

1.1.2. NCERC. As of 2022, NCERC is the sole remaining general-purpose critical experiments facility in the United States. NCERC maintains the infrastructure, expertise, personnel, and fissile material inventory to conduct an array of subcritical through prompt supercritical experiments. Many of the experiments conducted thus far in its decade long existence are performed to validate neutron cross section data, aid in microreactor development and support criticality safety studies [5].

NCERC operates four critical assemblies: Planet, Comet, Flattop, and Godiva IV. Planet and Comet are light duty and heavy duty vertical lift assemblies respectively[6] [7]. In 2018 Comet was used to test the Kilowatt Reactor Using Stirling TechnologY (KRUSTY) reactor, the first ground test of a nuclear reactor for space applications by the United States since 1965 [8]. Flattop consists a fissile core of material placed on a pedestal surrounded by a one metric ton natural uranium reflector and is commonly used for benchmarking and replacement measurements [9]. Finally, Godiva IV is a fast burst assembly composed of approximately 65 kg of highly enriched uranium (HEU) and is often used for studies of super prompt critical behavior as well as irradiations and demonstrations [10].

In addition to critical assemblies, NCERC also performs hand stacking operations with subcritical masses of nuclear material known radiation test objects (RTOs). RTO operations are typically in support of nonproliferation, treaty verification, safeguards, emergency response, and criticality safety studies. Unlike critical assembly operations, these configurations are created by hand and have multiplications from near 1 to about 20 ($k_{\text{eff}} = 0.95$) [11].

1.2. BENCHMARKS

Well documented, high quality criticality experiments can go onto become benchmarks. Benchmarks support nuclear data and criticality safety communities by supplying integral cross section data that can be used in validation efforts. These benchmarks are compiled in the International Criticality Safety Benchmark Evaluation Project (ICSBEP) handbook [12]. The ICSBEP handbook was started in 1992 by the United States Department of Energy and later in 1995 became an international project. Currently, the handbook is managed by the OECD (Organisation for Economic Co-operation and Development) NEA (Nuclear Energy Agency) and has seen contributions from 22 countries. The handbook consists of over five thousand subcritical, near critical, and critical experiments that have been performed around the world. As part of these evaluations, the precise geometries and material compositions of the experiment is recorded. These experiments can then be modeled by different computer simulations to evaluate their performance and estimate biases in computation tools and biases in nuclear data.

Benchmarks also provide integral neutron cross section data, or how a materials neutron cross section behaves over a continuous energy range. Differential cross sections on the other hand, are a material's cross section at discrete energies. Differential measurements are typically made at particle accelerators where precise neutron energies can be measured or by using time-of-flight methods at nuclear reactors beamports. Differential cross section data is compiled into nuclear data libraries such as the Evaluated Nuclear Data File (ENDF) database [13]. The differential data can then be validated by modeling benchmark experiments in codes such as Monte Carlo N-Particle® Code Version 6.2[1] (MCNP®6.2) and observing the differences between experimental and computational results.

[1]MCNP® and Monte Carlo N-Particle® are registered trademarks owned by Triad National Security, LLC, manager and operator of Los Alamos National Laboratory. Any third party use of such registered marks should be properly attributed to Triad National Security, LLC, including the use of the designation as appropriate. For the purposes of visual clarity, the registered trademark symbol is assumed for all references to MCNP within the remainder of this paper.

Criticality experiments can be designed such that their effective neutron multiplication factor (k_{eff}) is sensitive to a certain material's cross section, meaning small changes in the cross section have pronounced effects on the k_{eff} of the system. This is particularly useful for nuclear data validation efforts where a small inaccuracy in the differential data can be essentially amplified by the system when comparing experimental and computational results. This helps to identify compensating errors in nuclear data.

1.3. SENSITIVITY ANALYSIS OF CRITICAL EXPERIMENTS

Sensitivity analysis can be described as the study of how small changes in the inputs of a model can be attributed changes in its output. In the context of benchmarks, the sensitivity analysis of nuclear data is used to understand how different nuclide-reactions pairs contribute to changes in k_{eff}. This is useful before and after the experiment is actually performed. As mentioned previously, experimenters can intentionally design critical systems to be sensitive to certain materials, energies, and reactions. Then, after the experiment is performed and a detailed, as built model is created, the difference between experimental and computational results (the bias) can be attributed to nuclear data inaccuracies.

A common method to establish this relationship is to take the derivative of the output by some input variable. This derivative-based approach can be derived for different numerical simulations [14]. The ratio between the ratio of change in these values is known as the "sensitivity coefficient" [14]. For a integral benchmark, the sensitivity of k_{eff} to some energy dependent cross section, σ is:

$$S_{k_{\text{eff}},\sigma} = \frac{dk_{\text{eff}}}{k_{\text{eff}}} \frac{\sigma(E)}{d\sigma(E)} \,. \tag{1.1}$$

Different materials and reactions elicit different effects on the magnitude and sign on this coefficient. For example, a fission interaction will always yield a positive sensitivity as the increase of the cross section will yield a higher probability of fission for each interaction

thus increasing the number of neutrons in a generation. Conversely, radiative capture cross section will always yield a negative number as an increase in the cross section increases the probability a neutron will be captured, thus removed from the system.

1.4. MOLYBDENUM BENCHMARK

1.4.1. Background. In 2020, Los Alamos National Laboratory (LANL), Y-12 National Security Site, and the French Institut de Radioprotection et de Sûreté Nucléaire (IRSN) submitted a joint integral experiment request proposal to the Department of Energy's Nuclear Criticality Safety Program (NCSP). The proposal outlined the need for a series of criticality experiments to help validate differential molybdenum cross section data. The "Advanced Nuclear Technology" group (NEN-2) at LANL was tasked with designing and performing these experiments at NCERC.

Upon design and completion of these experiments, the resulting experimental data will be used to create a new benchmark. This benchmark will be used by nuclear data evalutors to validate differential molybdenum data and will reduce uncertainty in calculations made by criticality safety engineers.

1.4.2. Molybdenum Nuclear Data. Accurate molybdenum data is essential for reactor modelling and criticality safety studies. New molybdenum differential cross section measurements have been made at Rensselaer Polytechnic Institute (RPI) in 2015 and are presently underway at the Japan Proton Accelerator Research Complex (J-PARC) [15] [16]. Measurements at RPI targeted isotopically pure samples of ^{95}Mo, ^{96}Mo, ^{98}Mo, and ^{100}Mo between 1 and 620 keV while the measurements at J-PARC are targeting isotopically pure samples of ^{95}Mo, ^{96}Mo, and ^{97}Mo between 0 and 600 eV. Table 1.1 contains abundance and cross section data on the stable isotopes of molybdenum [13].

The ICSBEP handbook contains few benchmarks that are sensitive to the molybdenum cross section. This gives nuclear data evaluators little information to work with when validating nuclear data of molybdenum. This is especially true in the intermediate and

Table 1.1. Stable Molybdenum Isotope Capture Cross Sections

	^{92}Mo	^{94}Mo	^{95}Mo	^{96}Mo	^{97}Mo	^{98}Mo	^{100}Mo
% Abundance	14.65	9.19	15.87	16.67	9.58	24.29	9.74
σ_t (0.0253 eV) [b]	0.020	0.013	14.00	0.595	2.100	0.130	0.199
Resonance Integral [b]	0.966	1.400	118.5	17.53	17.13	6.552	3.903
σ_f (14 MeV) [b]	0.001	0.001	0.001	0.001	0.001	0.001	0.001

thermal neutron energy regions, with two benchmarks sensitive to thermal molybdenum and only one sensitive to intermediate molybdenum as shown in Figure 1.1 [17]. In addition to this, many molybdenum benchmarks have large biases between experimental and computational k_{eff} results. A few selected ICSBEP molybdenum benchmarks are shown along with their respective biases between experimental and computational results using JEFF-3.1.1, JENDL-4.0, and ENDF/B-VII.1 nuclear data libraries in Figure 1.2 [18] [19] [20].This bias could be a result of low quality benchmarks and/or inaccurate molybdenum data [21].

This new series of molybdenum critical experiments can be used to provide nuclear data evalutors with more integral molybdenum data to help validate the new cross section measurements.

1.4.3. U-Mo Fuels. Many of the first research reactors built by the United States were designed to operate using highly enriched uranium (HEU). Later in 1978 due to HEU proliferation concerns, the United States Department of Energy began to work to convert the existing research reactor fleet to low enriched uranium (LEU) fuel. For many research reactors this was accomplished by using dispersion fuels (uranium fuel kernels dispersed in an aluminum matrix) or uranium silicide fuels. For higher power and higher flux research reactors, a new type of fuel had to be developed. Existing LEU fuels could not provide high enough uranium densities and melting temperatures to still operate [22].

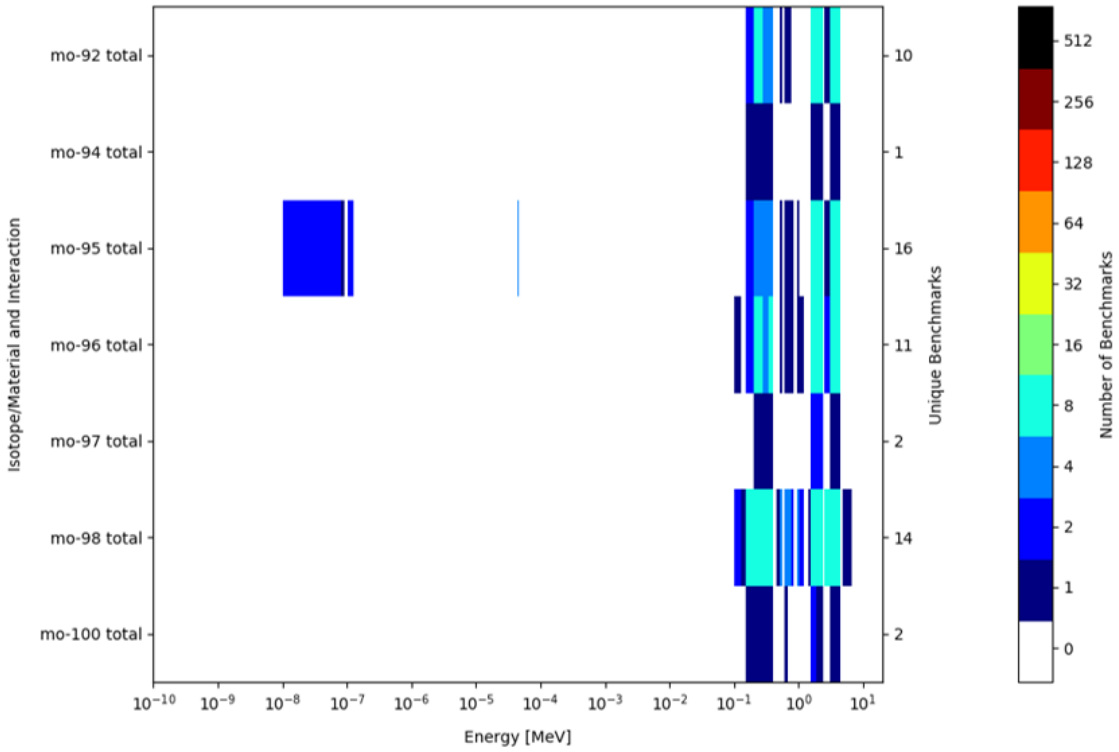

Figure 1.1. Molybdenum Sensitive Benchmarks

Since the 1990's uranium molybdenum (U-Mo) fuels have been the subject of many irradiation tests to meet this need [22]. Test elements of U-10Mo (LEU, 10wt.% Mo) are currently being irradiated at the Advanced Test Reactor (ATR) at Idaho National Laboratory [23]. Upon qualification of this new fuel, the remaining HEU fueled research reactors in the United States are slated to be converted to low enriched uranium (LEU) U-Mo fuel by 2030 [23].

In addition to research reactors, U-Mo fuels are a contender for space based fission reactors. The high uranium density of the fuel allows for more compact systems, an attractive option for space applications where smaller, lower mass systems are cheaper to launch into space. In 2018 successful tests of the Kilowatt Reactor Using Stirling TechnologY (KRUSTY) reactor were performed at NCERC. KRUSTY was a prototype space reactor that used a monolithic U-Mo as fuel [8].

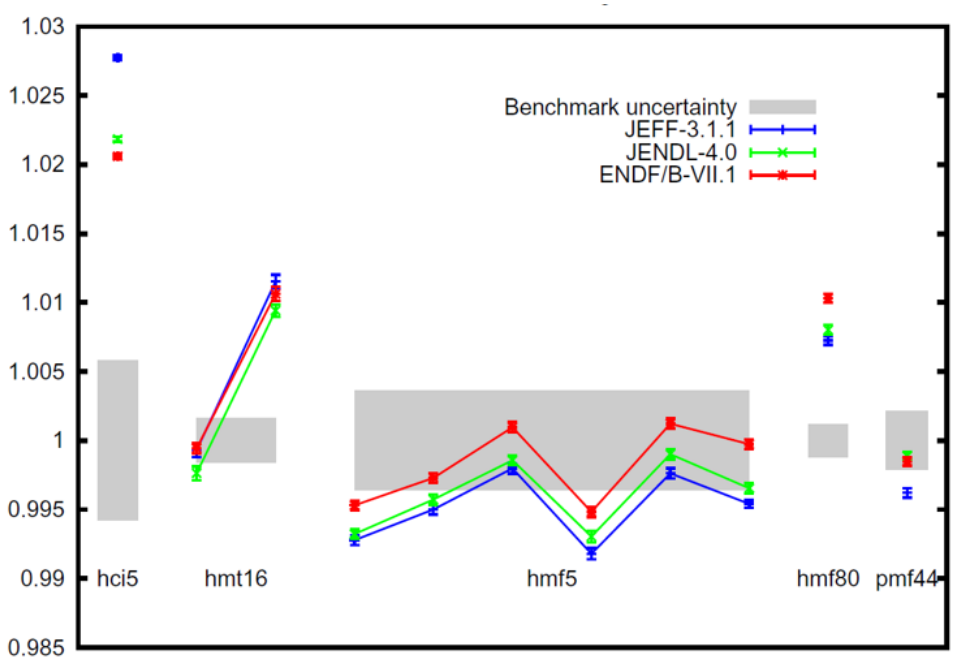

Figure 1.2. Bias in Molybdenum Benchmarks

1.4.4. Spent Nuclear Fuel. Many isotopes of molybdenum are common fission products for both U-235 and U-238. ^{95}Mo, a stable isotope of molybdenum, has a fission yield of 6.54% and 5.12% for U-235 and U-238 respectively in light water reactors. This, coupled with its strong intermediate capture cross section, makes it one of the 15 most absorbing fission products in light water reactors [16]. The isotopes total, elastic scattering, and radiative capture cross sections can be seen in Figure 1.3. For this reason, ^{95}Mo is used in criticality safety calculations for spent nuclear fuel. Quality nuclear data for intermediate ^{95}Mo is important to decrease the uncertainty in these calculations.

1.4.5. Structural Materials. Molybdenum is a common alloying agent in many types of stainless steel to improve corrosion resistance and high temperature performance. Stainless steel type 316 is commonly used core components of nuclear reactors and typically contains between 2-3% molybdenum. The use of TMZ, a titanium-molybdenum-zirconium alloy containing >99% Mo, has been demonstrated in molten salt reactors at temperatures in excess of 1300C [24].

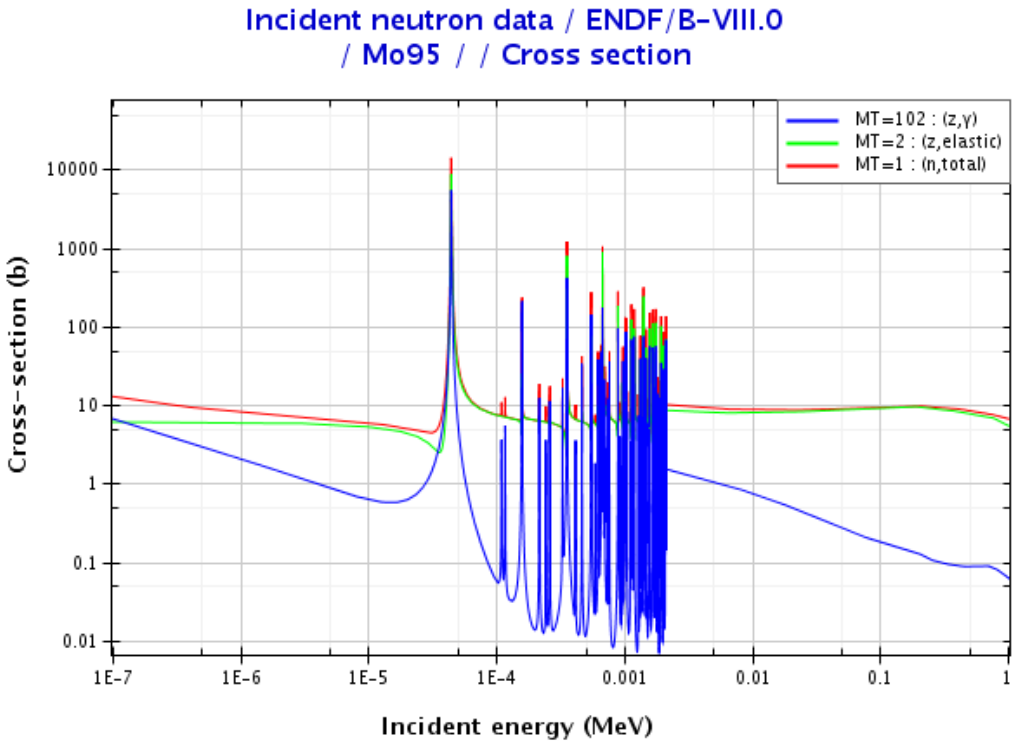

Figure 1.3. ^{95}Mo Cross Sections

1.5. PROJECT OBJECTIVE

The goal of this work is to present a more computationally efficient way to design optimized critical experiments than presently used methods.

Subsequent sections provide an overview of the computational techniques to model and perform sensitivity analysis on critical experiments. Then the conventional method of designing such an experiment is presented in Section 2.3, followed by a new method, employing particle swarm optimization. The theory and mathematical description of how this optimization method functions is presented in Section 3, and is coupled with MCNP6.2 in Section 4. Then in Section 5, a demonstration optimization is carried out to design the aforementioned molybdenum criticality experiments. The results from this optimization are then be compared to the conventional critical experiment design method in Section 6.

2. MONTE CARLO MODELLING AND SENSITIVITY ANALYSIS

2.1. MONTE CARLO N-PARTICLE TRANSPORT CODE

MCNP is a general-purpose Monte Carlo radiation transport that can be used to perform neutron transport simulations. By sampling and tracking generations of neutrons as they move and interact in a user-created three dimensional model, the code can calculate an eigenvalue for the system. As the name implies this is a Monte Carlo (stochastic) method that uses cross section libraries to determine the probability and how a neutron may interact with a material [25]. MCNP does not "solve" the transport equation, rather it simulates the physics that the transport equation describes. For eigenvalue problems a population of neutrons is sampled and their behavior is simulated from generation to generation until the process converges to a value. Due to an extensive amount of benchmarking and validation, MCNP serves as the method of choice for critical experiment designers and most criticality safety engineers.

To determine the probability a neutron of a given energy will interact with a material in the model, MCNP uses nuclear data libraries such as ENDF [13]. MCNP uses a free gas approximations for materials but can also use $S(\alpha, \beta)$ libraries for low energy neutrons where molecular and crystalline structure can effect neutron scattering [25].

In the benchmarking process, after a critical experiment is performed a high fidelity model is created and simulated in MCNP. This model includes precise geometric dimensions, isotopic makeups of materials, and temperatures. When simulated by MCNP, the calculated eigenvalue is typically slightly different than the experimental value. The difference between the two can be attributed to inaccuracies and uncertainties in nuclear data, as well as uncertainties in model parameters. By designing an experiment such that it is sensitive to a certain piece of nuclear data, more of this difference can be attributed to inaccuracies in nuclear data through further analysis.

2.2. ADJOINT-BASED SENSITIVITY K-EIGENVALUE COEFFICIENT

An adjoint-based k-eigenvalue sensitivity coefficient using a continuous-energy Monte Carlo radiation transport code was demonstrated and implemented into MCNP6 by Kiedrowski and Brown in 2013 [26]. This capability was verified using comparisons to analytical solutions, direct density perturbations and comparisons with other software.

2.2.1. Theory. As described in Section 1, the sensitivity coefficient for k_{eff} and a cross section σ of isotope j can be expressed as:

$$S_{k,\sigma} = \frac{dk}{k}\frac{\sigma_j}{d\sigma_j}\,. \tag{2.1}$$

The differential change in k from a differential change in some piece of nuclear data, can be derived using linear perturbation theory as [26]:

$$dk = -\frac{\langle \psi^\dagger, (d\Sigma_t - d\mathcal{S} - \lambda d\mathcal{F})\psi \rangle}{\langle \psi^\dagger, \lambda^2 \mathcal{F}\psi \rangle} \tag{2.2}$$

where ψ and $\psi^\dagger$ are the flux and its adjoint, $\lambda = 1/k$, Σ_t is the total macroscopic cross section, $\mathcal{S}$ is the integral scattering operator, and $\mathcal{F}$ is the integral fission operator [26]. By combining these equations we can get:

$$S_{k,\sigma} = \frac{\langle \psi^\dagger, \mathcal{P}^j_\sigma \psi \rangle}{\langle \psi^\dagger, \lambda \mathcal{F}\psi \rangle} \tag{2.3}$$

where $\mathcal{P}^j_\sigma$ is the perturbation operator defined as

$$\mathcal{P}^j_\sigma = (-N^j \sigma^j + \mathcal{S}^j_\sigma + \lambda \mathcal{F}^j_\sigma)\delta_g \delta_z \tag{2.4}$$

where N^j is the atomic density of isotope j, δ_g is equal to one if energy of neutron is within range g and zero otherwise, and δ_z is one if the neutron is within the region z and zero otherwise [26].

2.2.2. Nuclear Data Sensitivity Analysis with MCNP. As further demonstrated by Kiedrowski and Brown, MCNP6 can be used to calculate the adjoint-weighted tallies necessary to solve for the sensitivity coefficient [27].

The KSEN card was added to MCNP6.1 in 2013. The features allows the calculation of these nuclear data sensitivity coefficients [28]. For cross sections, isotope-reaction pairs and energy ranges of interest can be specified in the input file:

```
KSENn XS ISO=ZAID  RXN=MT  ERG=E0 E1
```

where ZAID references the isotope, RXN the reaction number, and ERG the energy range of interest. For example, the coefficient for a systems sensitivity to ^{238}U radiative capture below 1 eV can be expressed as:

```
KSEN1 XS ISO=92238.80c  RXN=102  ERG=0 0.000001
```

2.3. CONVENTIONAL CRITICAL EXPERIMENT DESIGN

The most common method to design these critical experiments is by conducting a parameter sweep. This is entails trying every combination of different experiment dimensions, masses, or concentrations in order to maximize some value, typically the sensitivity of the system to some piece of nuclear data. These calculations can be made in radiation transport codes such as Monte Carlo N-Particle Transport Code (MCNP) or SCALE [25] [29].

For some experiments this approach is quite reasonable. Take for example the most basic example of a sphere of fissile material surrounded by a polyethylene shell reflector. The experimenter only has one variable to adjust: only one reflector thickness exists such that the system is exactly critical. For example, one could simulate the system using every possible reflector thickness between zero and ten centimeters to the nearest millimeter. This is shown in Figure 2.1 and yields a total of 100 possible configurations to check.

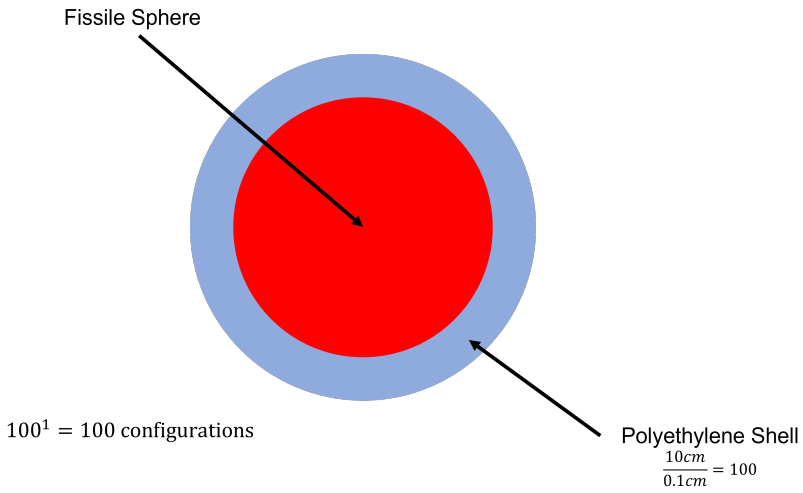

Figure 2.1. One Dimensional Example

Now let us consider a similar system but instead with a polyethylene shell followed by a tungsten shell reflector, two dimensions. What thicknesses of the inner and outer reflectors yield a critical system? This shown in Figure 2.2. If we were to once again check every reflector thickness for each shell between zero and ten centimeters to the nearest millimeter the total number of configurations becomes 100^2 or 10,000. Of this total, more than one critical configuration is likely to exist. We could then select the final choice based on some other desirable value such as a sensitivity or energy. Depending on the geometry and accuracy required, 10,000 combinations is still feasible with most modern computers, even using monte carlo methods, so this may still be a reasonable task to complete using the "brute force" approach.

Finally let us consider an example with three dimensions. Shown in Figure 2.3 is a sphere of fissile material surrounded by a shell of borated polyethylene and a shell of tungsten. What combinations of boron concentration, polyethylene thickness, and tungsten thickness exist such that the system is critical? Checking concentrations between zero and 10% to the nearest tenth and shell thicknesses between zero and ten centimeters to the nearest millimeter yields 100^3 or 1,000,000 configurations.

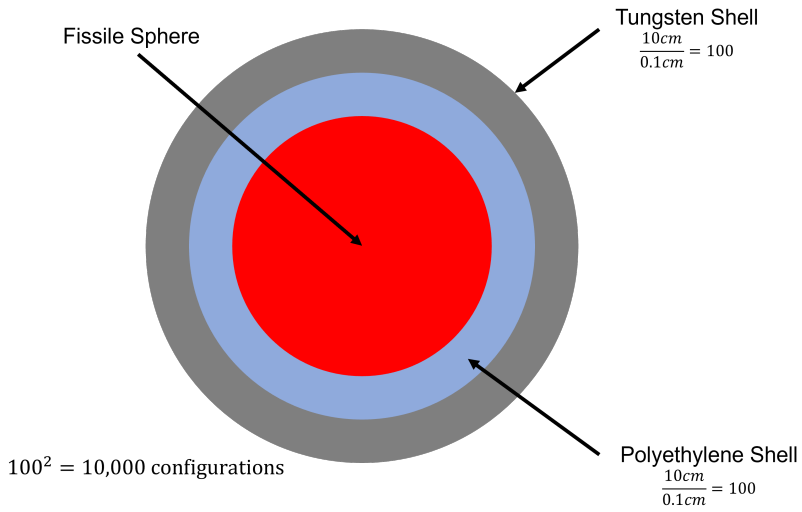

Figure 2.2. Two Dimensional Example

As additional dimensions are added, the total number of combinations increases exponentially. Even with the aid of modern high performance computing the computation time will become prohibitively long very quickly.

Depending on the ranges of the dimensions we check, many of these configurations are deeply subcritical or supercritical. Because of this, much of the computation time will be spent on configurations that are far from acceptable. Additionally, most modern computers would not be able to run 1 million monte carlo simulations in a reasonable amount of time. Is there a more computationally efficient method to identify these critical configurations? Furthermore, could a method be developed to also identify the most desirable of these critical configurations based on some other criteria?

This work demonstrates the development and application of an algorithm to produce these desirable configurations more efficiently than the conventional parameter sweep method.

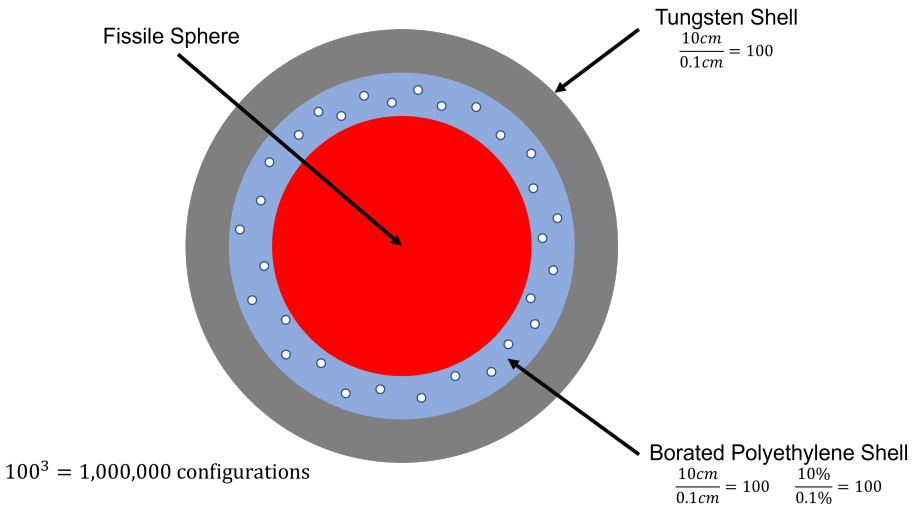

Figure 2.3. Three Dimensional Example

3. PARTICLE SWARM OPTIMIZATION

Particle swarm optimization (PSO) is a stochastic optimization method first proposed by Kennedy and Eberhart in 1995 [30]. The method was first inspired by how schools of fish and flocks of birds are able to work together to locate food. For example, rather than each bird looking bush to bush by itself to find food, each bird in the flock works together to share information about what is around them to more efficiently find the best bush. This swarm behavior can be implemented as an algorithm to locate optimal solutions on a search space.

3.1. THEORY

PSO works to locate the global optimum on the domain of a function. This domain is referred to as a "search space", where each point can be evaluated for a fitness. The global optimum, which could be the maximum or minimum of the search space depending on the goal of the optimization, is said to be the fittest location.

To achieve this, a population (swarm) of candidate solutions (particles) is randomly sampled throughout the search space. These particles move around the search space generation to generation until they converge on a point. The particles use a couple of pieces of information to dictate their movement on the search space. These include their individual best known and the entire swarms best known location on the search space. Once the swarm meets a set of user-defined convergence criteria, the algorithm is stopped and the swarms best known location is used as the optimal solution.

PSO is type of optimization method known as a metaheuristic. This means while it is not mathematically guaranteed to locate the global optimum of a search space, it requires very few assumptions about the problem. Unlike other optimization techniques such as

Newton's method and gradient descent, PSO does not require a differential form of the search space to exist, nor an analytical form. It requires no knowledge of the function itself other than its inputs and outputs.

Applications such as stochastic simulations are great candidates for this kind of optimization. Such programs like MCNP do not have an analytical description to perform derivative based optimization techniques.

3.2. MATHEMATICAL DEFINITION

For an n dimensional search space $\mathbb{R}^n$, the function to be optimized can be mapped to a single value $f : \mathbb{R}^n \rightarrow \mathbb{R}$. The algorithm begins by sampling S particles at random locations in the search space for the first generation. The function f, takes in the position of the i^{th} particle in the k^{th} cycle in the form of a vector, $\mathbf{x}_i^k \in \mathbb{R}^n$.

$$\mathbf{x}_i^k = \begin{bmatrix} d_1 \\ d_2 \\ \vdots \\ d_n \end{bmatrix} . \tag{3.1}$$

Upon calculating the fitness of each initial location, each particles best and the swarms best known locations are initialized as $\mathbf{p}_i^1$ and $\mathbf{g}^1$ respectively. For the k^{th} generation $\mathbf{p}_i^k$ and $\mathbf{g}^k$ position vectors are defined similarly to Equation 3.1. Each particle is then given a velocity that determines its position for the next generation. The velocity vector $\mathbf{v}_i^{k+1}$, for the i^{th} particle in generation $k+1$ is calculated by the following equation:

$$\mathbf{v}_i^{k+1} = \omega \mathbf{v}_i^k + \phi r_1 (\mathbf{p}_i^k - \mathbf{x}_i^k) + \rho r_2 (\mathbf{g}^k - \mathbf{x}_i^k) . \tag{3.2}$$

Random numbers r_1 and r_2, are distributed uniformly in (0,1) and the parameters ω, ϕ, and ρ are weights used to assign how much importance each term is given and are empirically tuned by the user. The first term can be thought of as the inertia of the particle while the second and third terms represent the contributions from the individual particles best known location and the swarms best known location respectively.

By adding the particles position vector with its newly calculated velocity vector, its new location can be given as:

$$\mathbf{x}_i^{k+1} = \mathbf{v}_i^{k+1} + \mathbf{x}_i^k \ . \tag{3.3}$$

The variables ω, ϕ, and ρ are known as the inertial, cognitive, and social weights respectively. Their values have a strong impact on how the swarm behaves over time. The inertial weight, ω determines how much the previous velocity will impact the next velocity. When this number is equal to or greater than one, the swarm will be unable to converge. The cognitive and social weights, ϕ and ρ, represent the weight of the acceleration of the particles towards the $\mathbf{p}_i^k$ and $\mathbf{g}^k$ values. If the social weight is larger than the cognitive weight, the particles will trend towards the swarm best more strongly than their individual best location. If either weight is too large, the particle may skip over the global optimum point and converge prematurely at a local optima. Similarly, if these weights are too small, it may take many generations for the swarm to converge.

Depending on the nature of the search space, different weights may cause the swarm to converge more efficiently. For example, a search space with many local optima will benefit from an algorithm with a higher cognitive value as this leads to particles exploring around them more thoroughly, at the cost of a slower convergence. Conversely, a problem with only one optima (also the global optima) may benefit from a higher social value as this leads to particles searching in the vicinity of $\mathbf{g}^k$ for a better solution.

3.3. ANALYTICAL EXAMPLES

3.3.1. Rosenbrock Function. To demonstrate the swarm behavior with different parameter weights, an example optimization will be conducted on a test function. The Rosenbrock function, commonly used as a performance test for optimization algorithms, is a non-linear uni-modal function with a single global minima [31]. In its n-dimensional form it takes the form of:

$$f(\mathbf{x}) = \sum_{i=1}^{n-1} [100(x_{i+1} - x_i^2)^2 + (1 - x_i)^2] \,. \tag{3.4}$$

Although PSO algorithms can operate in n-dimensional search spaces, for visual simplicity this optimization will use Equation 3.4 in its two dimensional form where $n = 2$. This optimization will attempt to locate the global minimum which is located at $f(1, 1)$ using a variety of different weight combinations to demonstrate their effects on the swarms behavior over time. To demonstrate the impacts of these weights when taken to the extremes, a few toy examples are shown below.

Figure 3.1 shows the evolution of a low cognitive weight swarm on the Rosenbrock function. The swarm was able to locate the valley but not its minimum point. The swarm converged around $f(0.7, 0.5)$ rather than the global minimum at $f(1, 1)$. The low cognitive weight leads to particles to converge quickly without thoroughly exploring the search space.

Figure 3.2 shows the evolution of a swarm with a low social weight. Since the particles are only attracted to their best known location, they quickly become 'stuck' at that point. This is because as contributions from the inertial and cognitive terms of their velocity decreases from generation to generation the total velocity approaches zero.

Figure 3.3 shows the evolution of a swarm with a inertial weight equal to one. As mentioned previously, if the inertial weight is equal to or greater than one particles will not be able to "slow down" as all of the velocity from the previous generation is being added to the next generations. This prevents the particles from converging.

Lastly, Figure 3.4 shows the evolution of a swarm with empirically tuned weights. This combination of weights allowed the swarm to converge on the global minimum at $f(1,1)$. Swarms on search spaces with a single global optima tend to perform better with higher social weights [32].

3.3.2. Rastrigin Function. To demonstrate the swarm behavior on a search space with many local optima, an example optimization will be conducted on another test function. The Rastrigin is a non-linear multi-modal function with many local minima [33]. In its n-dimensional form it takes the form of:

$$f(\mathbf{x}) = 10n + \sum_{i=1}^{n} [x_i^2 - 10\cos 2\pi x_i] \,. \tag{3.5}$$

Figure 3.5 shows the evolution of a swarm with a low cognitive weight. The particles are attracted only to the swarm best and are unable to explore their own best known locations since ϕ is set equal to zero. This caused the swarm to quickly converge on a local minimum rather than the global. This is particularly an issue for optimizing multimodal functions such as the Rastrigin function.

Figure 3.6 shows the evolution of a low social weight swarm on the same function. The lack of any social weight prevents any communication between the particles, causing the particles to quickly become stuck near their starting positions.

Figure 3.7 shows the evolution of a high inertial weight swarm. As explained previously, any swarm with an inertial weight equal to or greater than one cannot converge. The particles retain all of their velocity from the previous generation meaning they can never slow down.

Lastly, Figure 3.8 shows the evolution of a swarm with empirically tuned weights. This combination of weights allowed the swarm to converge on the global minimum at $f(0,0)$. For this search space a low inertial weight was found to be effective as it lead to a lower velocity particle as this helps the particles not skip over the many local minimum of the Rastrigin function.

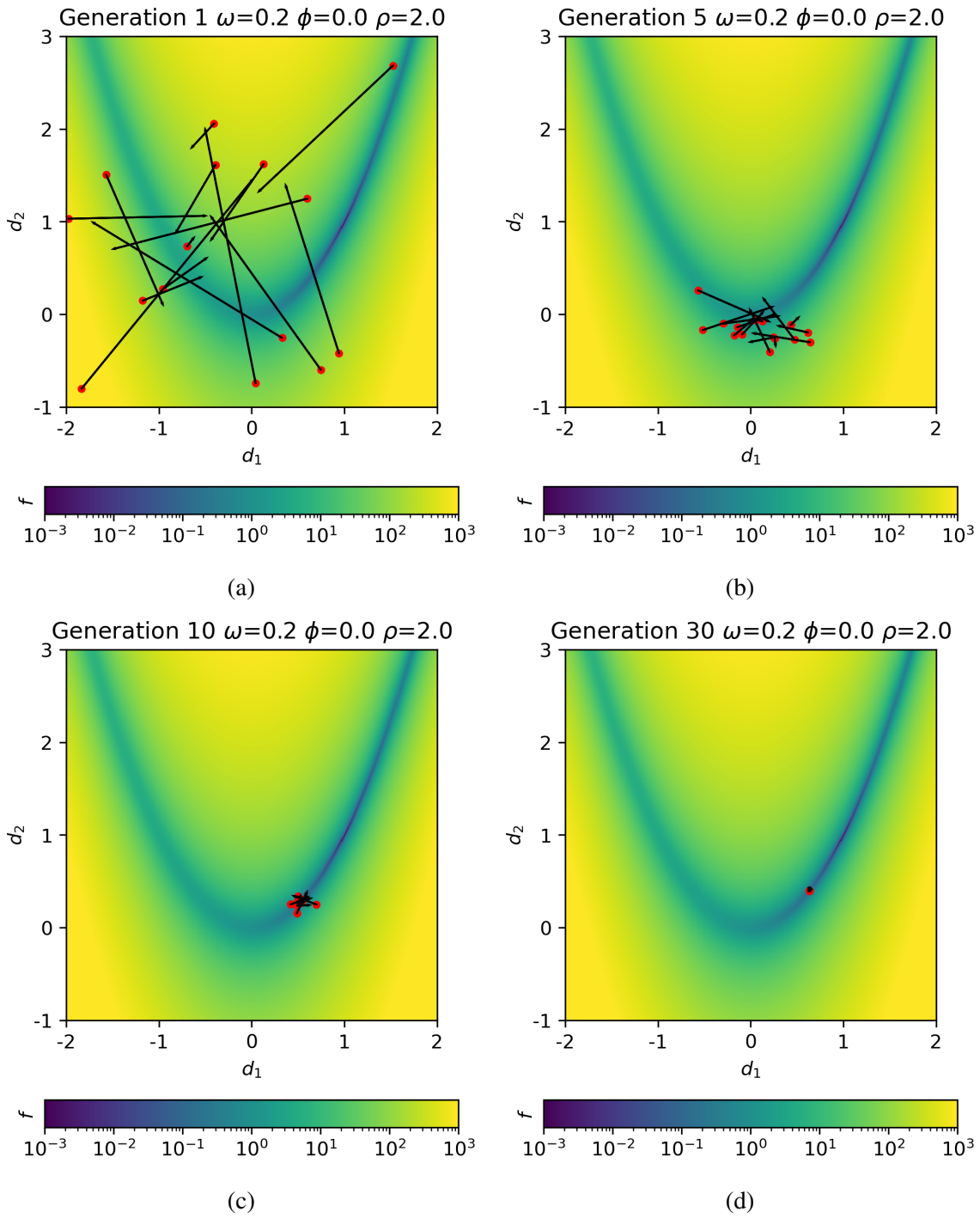

Figure 3.1. 2-D Rosenbrock Function with Low Cognitive Weight Swarm

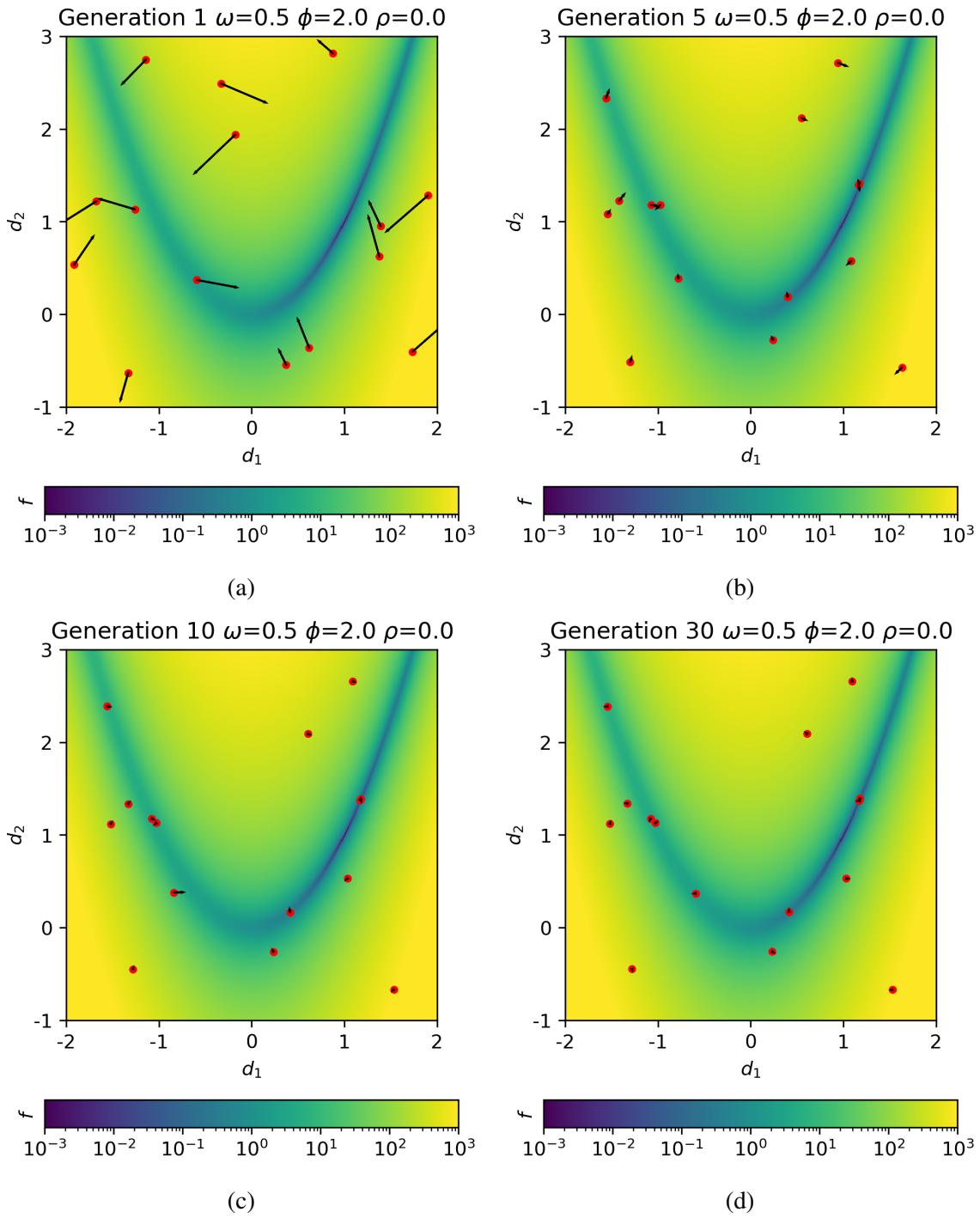

Figure 3.2. 2-D Rosenbrock Function with Low Social Weight Swarm

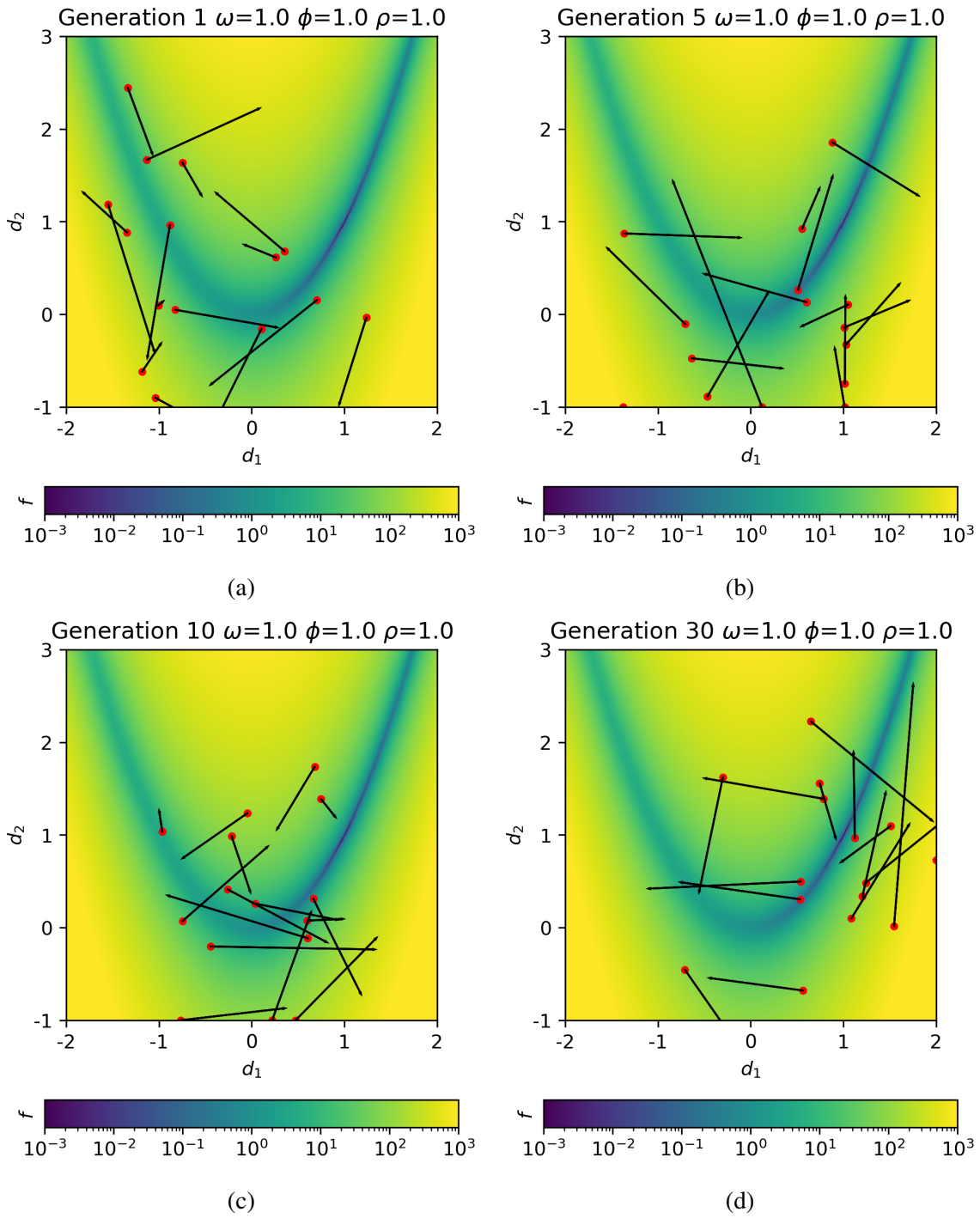

Figure 3.3. 2-D Rosenbrock Function with High Inertial Weight Swarm

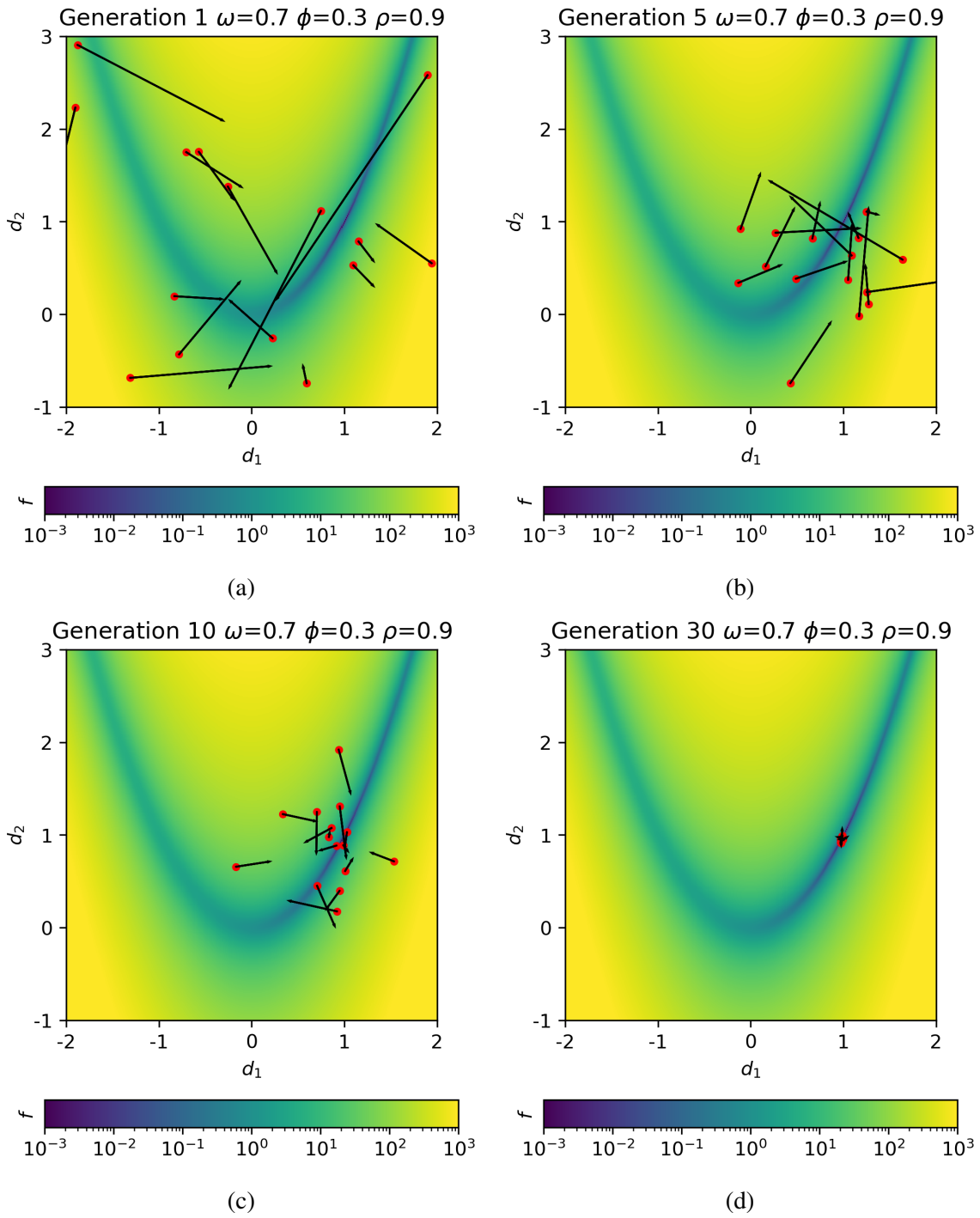

Figure 3.4. 2-D Rosenbrock Function with Tuned Weight Swarm

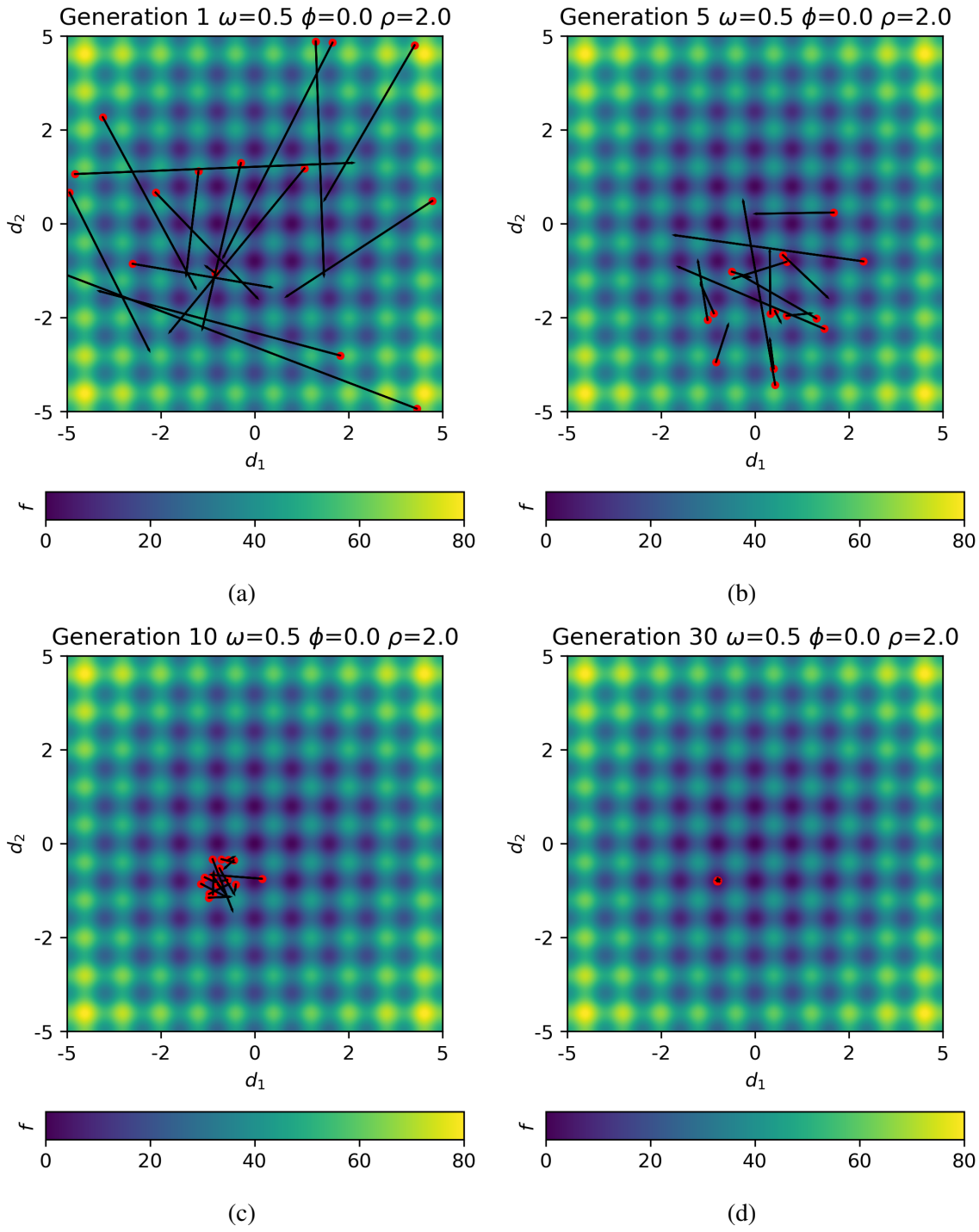

Figure 3.5. 2-D Rastrigin Function with Low Cognitive Weight Swarm

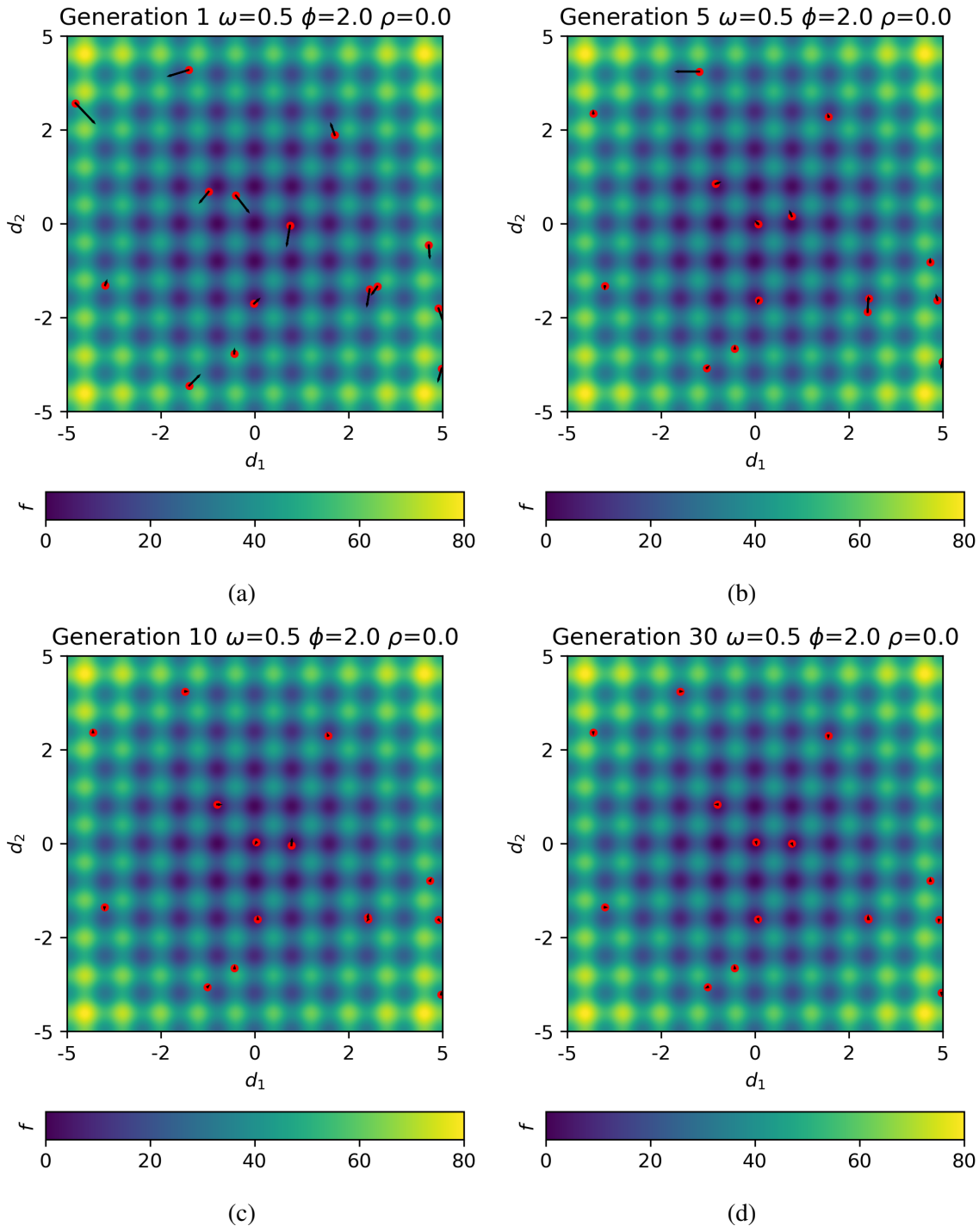

Figure 3.6. 2-D Rastrigin Function with Low Social Weight Swarm

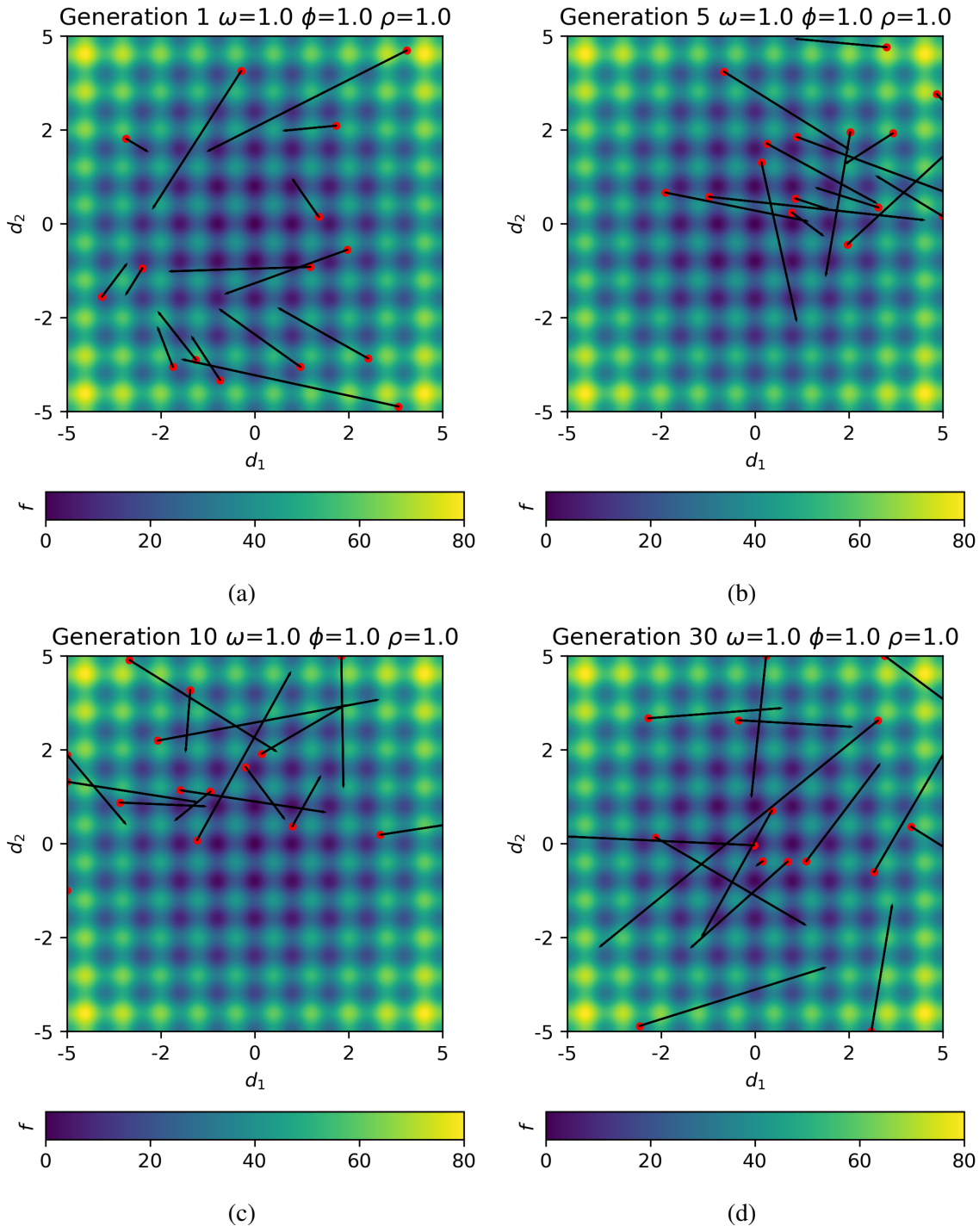

Figure 3.7. 2-D Rastrigin Function with High Inertial Weight Swarm

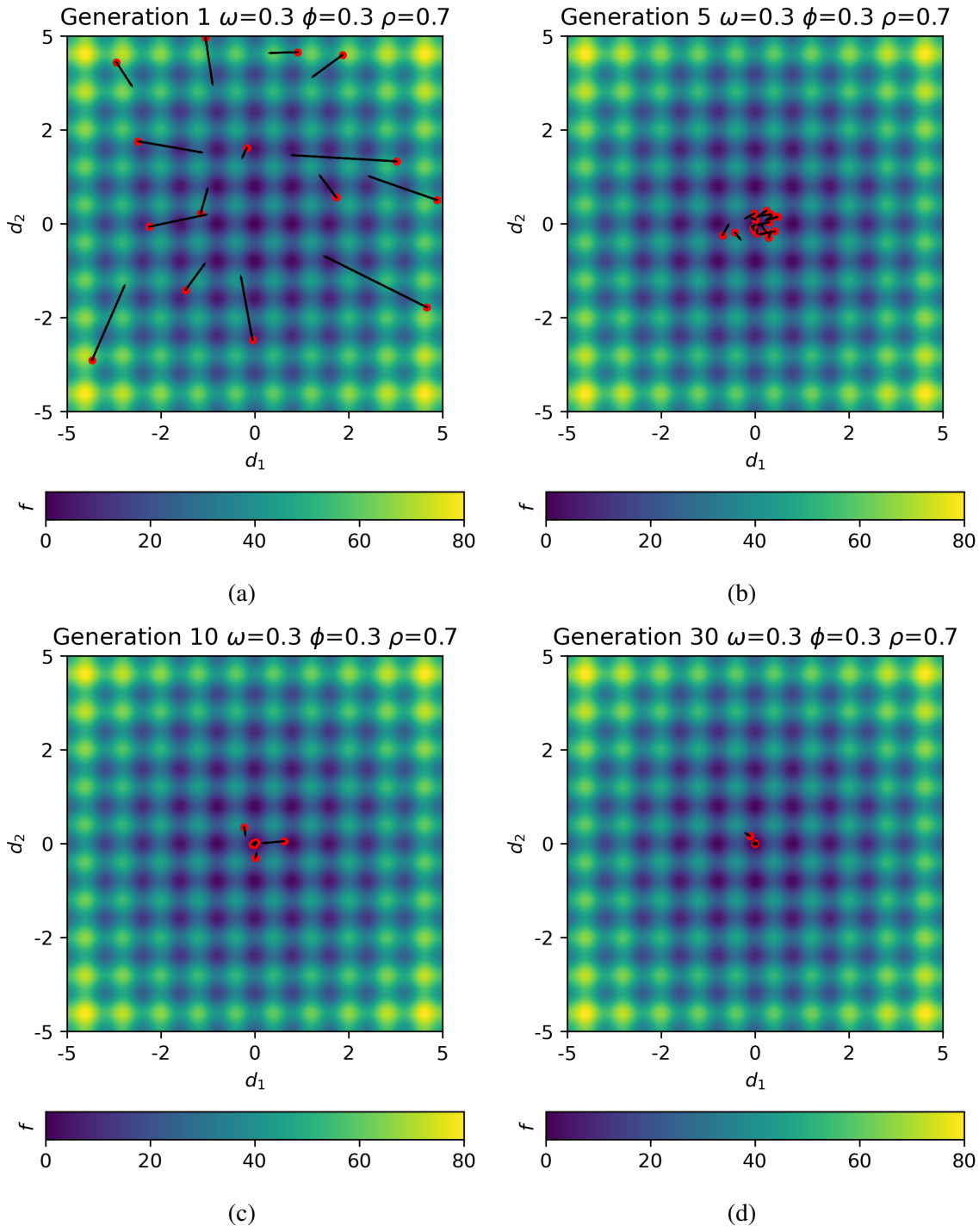

Figure 3.8. 2-D Rastrigin Function with Tuned Weight Swarm

4. MCNP-PSO ALGORITHM

To apply particle swarm optimization to the design of critical experiments, a MCNP-PSO coupled algorithm was developed using Python [34], a general-purpose programming language. The algorithm generates particles on a user-defined search space of experiment parameters, such as thicknesses or material concentrations, and generates MCNP inputs based on their location in the search space. MCNP then runs these inputs and each particle's fitness is presented as a function of some parameter in its output such as a sensitivity or energy. As MCNP input and output files can be read by any text editor, Python can be used to write and inputs and read outputs.

4.1. INITIALIZATION

To begin, the user presents the algorithm with a reference MCNP input file that they wish to be optimized, the parameters of the input they wish to perturb, and the value that they want to be optimized. To constrain the search space, the user specifies the range over which each input parameter can be perturbed (e.g. reflector thickness between zero and five centimeters).

4.2. SEARCH SPACE SAMPLING

Once the search space has been defined, the next step is to sample locations for each particle's initial location. If the swarm size is not sufficiently large, sampling purely random starting locations can lead to poor coverage of the search space. It has instead been shown effective to utilize near-random sampling methods. This algorithm uses a statistical technique known as Latin hypercube sampling (LHS) [35].

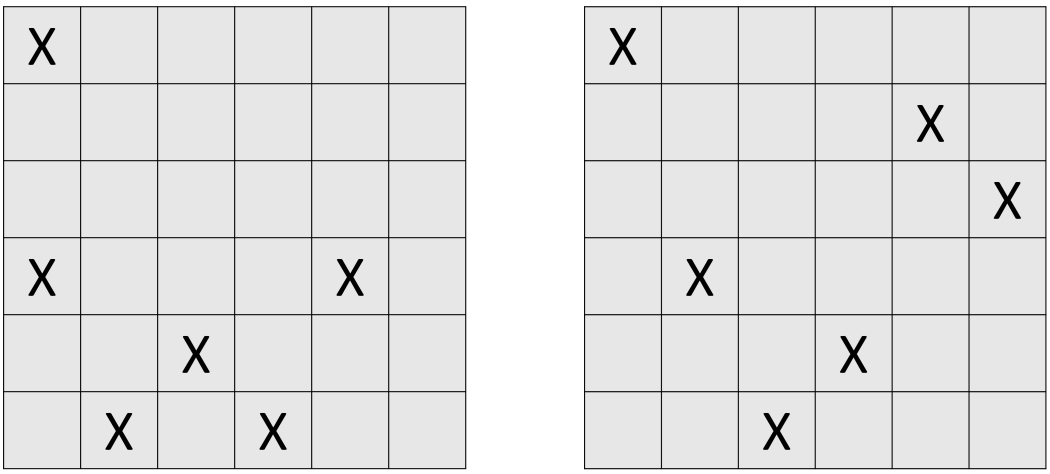

(a) (b)

Figure 4.1. Random (a) and LHS (b) Sampled Search Spaces

For a swarm of S particles on a search space of n dimensions, each dimension d_n, is partitioned in to S groups. Each of these partitions is randomly sampled one time. Particles are placed at random combinations of these partitions, this ensures each dimension is evenly sampled. For a two-dimensional case with a swarm size of six particles, the search space is partitioned into six columns and six rows. Each row and column is sampled once. An exampled of a purely randomly sampled and LHS sampled search space is seen in Figure 4.1. The purely randomly sampled space (a) some partitions of the search space are left unsampled, while all partitions are sampled once in the LHS sampled space (b).

The initial velocities of each particles is set to a vector with a random direction. To ensure the initial magnitude is does not cause the particle to leave the search space, its value is selected to be a random number between the upper and lower limits of each dimension of the search space. The initial velocity of the i^{th} particle is notated as $\mathbf{v}_i^1$.

4.3. INPUT GENERATION AND EVALUATION

Upon sampling the search space, an MCNP input file is created for each particle location. This is accomplished by altering the reference input file provided by the user. Once an input is created corresponding to each particle location, they are evaluated in MCNP. Using the output file from each location, the particles fitness can be determined.

For a candidate solution to be considered as an option for selection it must be near-critical. Solutions are considered "near-critical" if their k_{eff} is within 1000pcm (percent milli-k) of critical. MCNP will calculate the k-eigenvalue of each input using the KCODE and KSRC source cards. This will provide configurations very close to critical that will serve as a starting point for further evaluation. As demonstrated in the ICSBEP handbook, the bias between experimental and computational k_{eff} can often exceed 1000pcm depending on the neutron energy spectrum, materials used in the system and other parameters.

With this in mind, the algorithm must rank near-critical systems more fit than subcritical and supercritical systems. Of the near-critical systems, they must then be ranked by the optimization parameter of the users choice. For example, this could include an energy integrated cross section sensitivity using the KSEN card, energy of the average neutron lethargy causing fission (EALF), or percent of fissions in a given energy range. All of these values can be determined by MCNP for each particle location.

For example, the fitness of the i^{th} particle in the k^{th} generation can be expressed as:

$$f(\mathbf{x}_i^k) = \begin{cases} |A| & 0.99 \leq k_{eff} \leq 1.01 \\ -|k_{eff} - 1| & otherwise \end{cases} \tag{4.1}$$

where A is the value to be maximized.

4.4. MOVING PARTICLES

Now that we have initialized particles at pseudo-random positions in the search space, their initial velocities, and have a method of evaluating their fitness, we now must move them according to Equation 3.2 and 3.3. This process of calculating the new elements of a particles velocity $\mathbf{v}_i$ and position vectors $\mathbf{x}_i$ and updating particle bests $\mathbf{p}_i$ and the swarm best $\mathbf{g}$ positions is described by Figure 4.2.

```
for each particle i = 1, 2, ... S:
  for each dimension d = 1, 2, ... n:
    generate random numbers: r1, r2 ∈ (0, 1)
    update particle's velocity: v_i^{k+1} = ωv_i^k + φr1(p_i^k − x_i^k) + ρr2(g^k − x_i^k)
  update the particle's location: x_i^{k+1} = x_i^k + v_i^{k+1}
  if f(x_i^{k+1}) > f(p_i^k):
    update particle's best known position: p_i^{k+1} = x_i^{k+1}
    if f(x_i^{k+1}) > f(g^k)
      update swarms's best known position: g^{k+1} = p_i^{k+1}
```

Figure 4.2. Algorithm for Updating Particle Velocities

The inertial, cognitive, and social weights as well as the number of particles in the swarm is also specified by the user. Using knowledge of what the search space may look like these weights can be tuned to optimize the performance of the algorithm. As demonstrated in Section 3.3, swarms with high social weights tend to perform better on spaces with a single global optima, while swarms with higher cognitive weights tend to perform better on spaces with many local optima. If no assumptions about what the search space can be made, a conservative approach is to sample more particles.

The number of particles sampled heavily effects the amount of time it will take the swarm to converge. This is simply because the more particles there are, the more inputs MCNP must evaluate per generation. The amount of time it takes to the algorithm calculate velocity and positions is negligible compared to the amount of time MCNP takes to simulate the configuration.

4.5. CONVERGENCE CRITERIA

Particles are moved, their positions evaluated, and bests updated until a set of convergence criteria are met. For this algorithm the swarm is said to be converged if and only if:

$$\frac{1}{S}\sum_{i=1}^{S} f(\mathbf{p}_i) > 0.95 f(\mathbf{g}) \tag{4.2}$$

The means that once the average particle best is within 5% of the swarm best the algorithm with terminate. At this point, the swarm best location $\mathbf{g}$ is taken to be the optimum location identified by the algorithm on the search space. Depending on the computational resources or time available, this value can be increased or decreased to achieve a higher or lower degree of convergence.

5. MOLYBDENUM CRITICAL EXPERIMENT OPTIMIZATION

5.1. OPTIMIZATION OBJECTIVE

To make a critical experiment valuable to nuclear data evalutors, the system should be as sensitive as possible to the isotope-reaction pair of interest. As the sensitivity is energy dependent, we can design different configurations to target different neutron energy regimes.

The NCSP proposal from Section 1.4.1 specifically mentions the ^{95}Mo radiative capture cross section as an isotope reaction pair that needs validation due to disagreements in its cross section between major nuclear data libraries as well as its large effect on k_{eff} in some nuclear systems. As discussed earlier, ^{95}Mo has the largest cross section of any stable isotope of molybdenum and boasts a 5,000 b resonance at 44.5 eV.

To achieve sensitives to all parts of the neutron energy spectrum, three unique critical configurations with two types of fuel will be used to target different energies of interest. As shown in Table 5.1, a thermal case (<0.625 eV), an epithermal case (0.625 eV - 2 keV), and a unresolved resonance region (URR) (2 - 200 keV) will be optimized for both uranium and plutonium systems. This yields a total of six energy sensitivity optimized critical configurations the PSO algorithm will produce. The algorithm will use the KSEN card in MCNP to calculates these energy integrated sensitivities to the ^{95}Mo radiative capture cross section.

Table 5.1. Energy Ranges of Interest

Range	E_L	E_H
Thermal	0 eV	0.625 eV
Epithermal	0.625 eV	2 keV
URR	2 keV	200 keV

The sensitivity of k_{eff} to the ^{95}Mo capture cross section in different energy ranges can be expressed by integrating Equation 5.1 over the bounds of that energy range.

$$S_{k_{eff},\sigma(E_L,E_H)} = \int_{E_L}^{E_H} \frac{dk_{eff}}{k_{eff}} \frac{\sigma(E)}{d\sigma(E)} dE \,. \tag{5.1}$$

Substituting A for this sensitivity into Equation defines the fitness of each particle:

$$f(\mathbf{x}_i^k) = \begin{cases} |S_{k_{eff},\sigma(E_L,E_H)}| & 0.99 \leq k_{eff} \leq 1.01 \\ -|k_{eff} - 1| & otherwise \end{cases} \tag{5.2}$$

5.2. URANIUM MOLYBDENUM CRITICAL EXPERIMENT

This series of uranium molybdenum critical experiments will be used as an demonstration two-dimensional optimization. The results of this optimization will then be compared to the conventional parameter sweep method.

5.2.1. Comet Vertical-Lift Assembly. The Comet assembly will be used to conduct the uranium molybdenum critical experiments. This assembly is currently located at NCERC and operated by Los Alamos National Laboratory. Comet has been used in hundreds of critical experiments since the 1950's to support criticality safety and nuclear data studies [7] [4]. The assembly is composed of a upper stationary and lower movable platform upon each a subcritical mass is placed. As the lower platform is raised, the two subcritical masses get closer together, increasing the reactivity of the system.

The upper stationary platform on Comet can accommodate 20,000lbs while the lower movable platform can accommodate 2,000lbs. This allows experimenters flexibility to construct a wide arrangement of systems using heavy reflectors, moderators, and fissile materials.

An array of nuclear instrumentation including He-3 neutron detectors and compensated ion chambers are used to monitor the neutron population leaking from the system. Operators can use this information to position the lower platform such that the system is critical or very slightly supercritical using the reciprocal neutron multiplication method (1/M) as a function of separation distance. The lower movable platform is able to be positioned with an accuracy of one mil (one thousandth of an inch).

5.2.2. Reference Geometry. The uranium molybdenum critical experiments will use Jemima plates as fuel. These are thin HEU metal plates with a diameter of 53.35cm and a thickness of 3mm. Single Jemima plates will be stacked with polyethylene and molybdenum plates to create a fuel unit as seen in Figure 5.2. Twelve of these units will be stacked inside a copper reflector as seen in Figure 5.3. By varying the polyethylene and the molybdenum plate thicknesses, the neutron energy spectrum of the system can be altered as well as the sensitivity to the ^{95}Mo capture cross section. This is a similar form to the Zeus experiments performed on Comet, which went on to become benchmarks [36] [37]. A photograph of the Comet assembly with the Zeus experiments is seen in Figure 5.1. A generic MCNP input of this reference geometry can be found in Appendix A.

5.2.3. Search Space and Swarm Characteristics. For this optimization the input parameters for our PSO algorithm, d_1 and d_2, become the polyethylene and molybdenum plate thicknesses.

The limits of a search space are difficult to select without any a priori knowledge of the system. It is reasonable to select the lower limits of our dimensions as zero, but what about the upper limit? Defining an upper limit too low might result in creating a search space that doesn't contain the global optima. Although selecting an upper limit too large leads to the swarm to be sampled over a region of the search space exceedingly far from the optima, as seen in Equation 3.2, the further a particle is from the swarm best, the

Figure 5.1. Comet Assembly with Zeus Experiment

more they are pulled toward it. This means, particles that are sampled in deeply subcritical or supercritical regions will be strongly attracted towards more near-critical regions of the swarm space.

The upper limit of the search space for both dimensions will be set to 5.0 cm with a 0.5 mm resolution. This is equal to $10,000$ possible configurations. If additional critical configurations are identified outside of this region, these limits can simply be raised and the algorithm ran again.

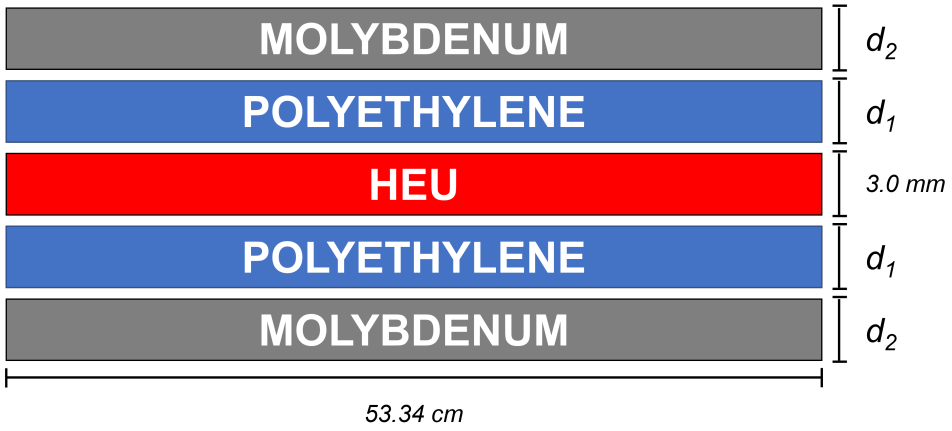

Figure 5.2. Uranium Fuel Unit

Table 5.2. Uranium Search Space

Dimension	Min [cm]	Max [cm]	Partition [cm]
d_1 (Polyethylene)	0.0	5.0	0.05
d_2 (Molybdenum)	0.0	5.0	0.05

Similarly to the limits, it is difficult to select swarm characteristics without a priori knowledge. However we can make some deductions using simple assumptions that will help us make these selections. Knowing that molybdenum acts as a neutron poison, in general, the thicker the molybdenum, the lower k_{eff} will be. With that, there should be a single line of critical configurations that divides subcritical and supercritical. On this line of critical configurations, configurations with more polyethylene should be more thermal and ones with less should be faster. As our sensitivity of interest is energy integrated, the optimal will lay on that critical line depending on what the energy range of interest is. To one side of the line the system will be too thermal, on the other it will be too fast.

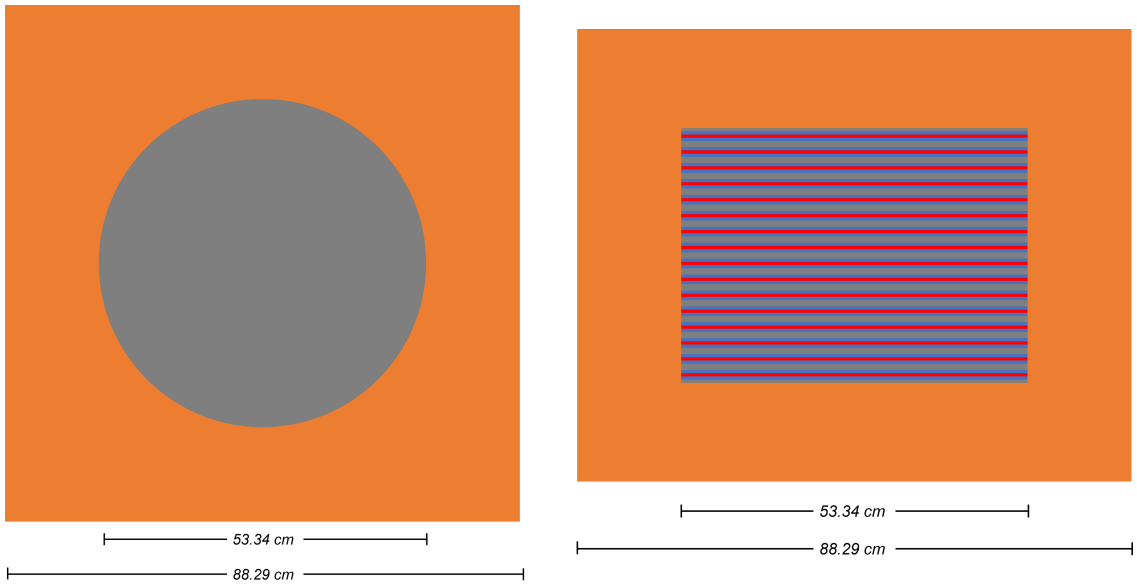

Figure 5.3. Plan and Profile View of Stacked Fuel Units in Copper Reflector

From this we can assume there will be a single optima on this critical line. We can further say that the function likely looks something like the Rosenbrock function: a valley with a single optima. From previous discussion, we know that swarms with higher social weights tend to perform better on functions with a single global optima. The selected swarm characteristics for this optimization are seen in Table 5.3.

The results from this optimization are presented in Section 6.1. Knowing the search space contains a total of 10,000 possible configurations, we will be able to compare the total number of configurations checked by the algorithm before it converges. This will allow us to calculate how much faster the algorithm was than an equivalent parameter sweep would be.

Table 5.3. Uranium Swarm Characteristics

S	ω	ϕ	ρ
15	0.5	0.6	0.9

5.3. PLUTONIUM MOLYBDENUM CRITICAL EXPERIMENT

This series of plutonium molybdenum critical experiments will be used as an demonstration three-dimensional optimization. This results of this optimization will then be compared to the conventional parameter sweep method.

5.3.1. Planet Vertical-Lift Assembly. The Planet assembly will be used to conduct the plutonium molybdenum critical experiments. This assembly is also currently located at NCERC and operated by Los Alamos National Laboratory. Planet is a vertical-lift assembly that operates in a similar fashion to Comet. Planet however, is smaller and is commonly used for lower mass critical experiments [6]. A photograph of the Planet assembly is seen in Figure 5.4.

5.3.2. Reference Geometry. The plutonium molybdenum critical experiments will use aluminum stabilized delta phase plutonium plates clad in stainless steel as fuel. These plates were originally used in the Zero Power Physics Reactor (ZPPR) at Idaho National Laboratory and are referred to as the ZPPR plates [38]. These plates measure 7.62 cm by 5.08 cm by 0.3175 cm [39]. Similar to the Jemima plates, the ZPPR plates have been used in many criticality experiments and are geometrically and isotopically well characterized. Simplified dimensions and the chemical make up of the fuel can be seen in Tables 5.4 and 5.5. A generic MCNP input of this reference geometry can be found in Appendix B.

Table 5.4. ZPPR Plate Specifications

Dimensions (cm)	^{239}Pu (g)	^{240}Pu (g)	^{241}Pu (g)	^{242}Pu (g)	^{241}Am (g)	Al (g)
7.62 x 5.08 x 0.3175	98.98	4.716	0.208	0.0049	0.2482	1.128

Table 5.5. ZPPR Plate Cladding Thicknesses

Front (cm)	Back (cm)	Sides (cm)	Top and Bottom (cm)
0.0305	0.1474	0.0508	0.2985

These plates will be stacked in a 6 by 4 array, which in total measures about 30 cm by 30 cm. On top of this layer of fuel a molybdenum and a polyethylene plate of similar area will be stacked. Similar to the uranium configurations, this stacking of fuel makes up a single fuel unit and the molybdenum and polyethylene thicknesses will served as the d_1 and d_2 dimensions for our optimization. The stack of fuel units will be surrounded by a polyethylene reflector. The thickness of this reflector in the axial and radial directions will serve as the d_3 dimension for this optimization. The fuel unit and fuel stack can been seen in Figures 5.5 and 5.6.

Figure 5.4. Planet Assembly

5.3.3. Search Space and Swarm Characteristics. For this optimization the input parameters for our PSO algorithm, d_1, d_2, and d_3, become the polyethylene plate, molybdenum plate, and reflector thicknesses respectively. As discussed previously, a two-dimensional optimization should yield a single critical line. Therefore, we can assume that this three-dimensional optimization will yield a critical surface. Each point on this surface represents a combination of our three dimensions that yields a critical configuration. Once

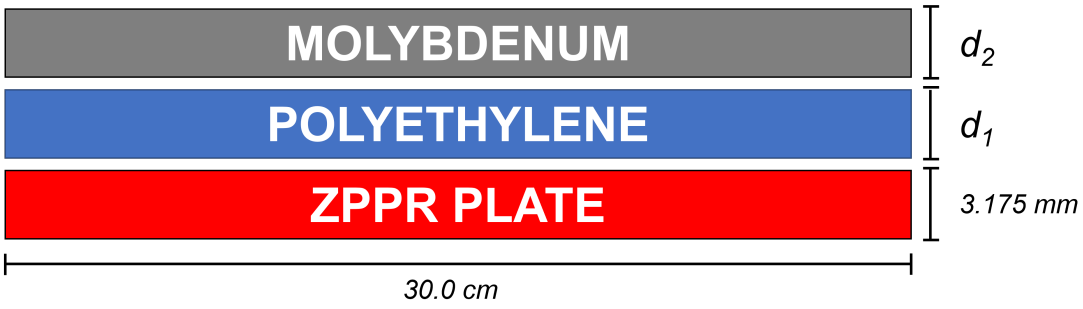

Figure 5.5. Plutonium Fuel Unit

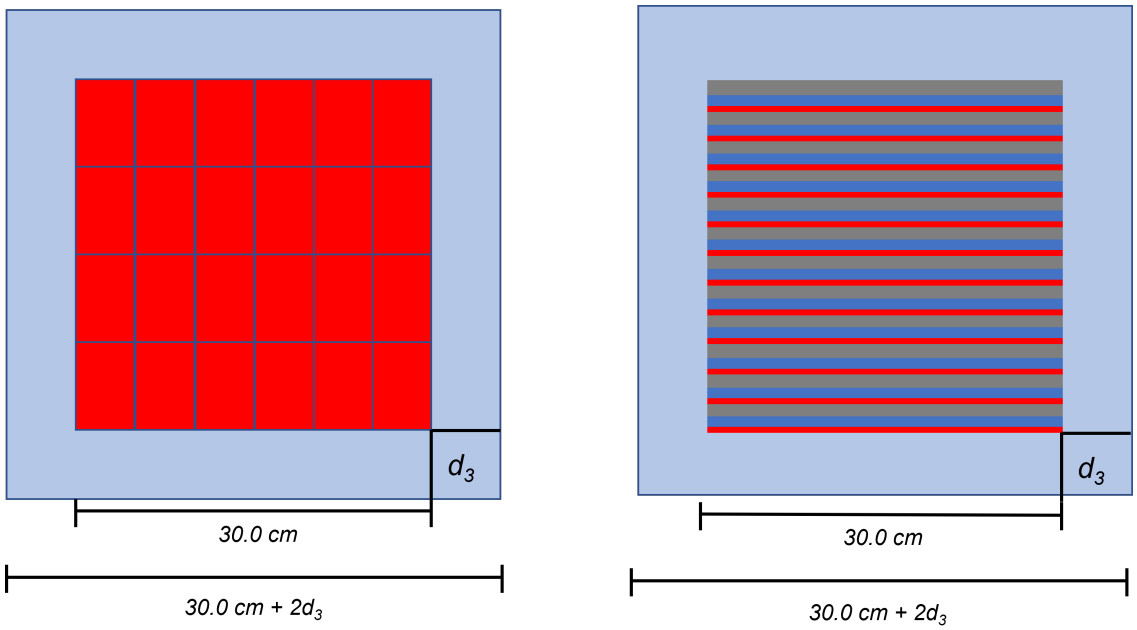

Figure 5.6. Plan and Profile View of Stacked Fuel Units in Polyethylene Reflector

again, the algorithm will work to identify a point on this surface that maximizes the sensitivity to the ^{95}Mo capture cross section in a given energy range. The limits of the search space can be seen in Table 5.6 and contains $4,000,000$ possible configurations. Once again, if additional critical configurations are identified outside of the search space, the dimensions in Table 5.6 can be increased accordingly.

Table 5.6. Plutonium Search Space

Dimension	Min [cm]	Max [cm]	Partition [cm]
d_1 (Polyethylene)	0.0	10.0	0.05
d_2 (Molybdenum)	0.0	2.5	0.05
d_3 (Reflector)	0.0	20.0	0.05

Similar to the previous optimization, this search space should also contain a single global optima. For this reason the same inertial, cognitive, and social weights will be used as the previous optimization. Since this search space is larger than previous, a swarm of 25 particles will be used. The swarm characteristics for this optimization can be seen in Table 5.7.

Table 5.7. Plutonium Swarm Characteristics

S	ω	ϕ	ρ
25	0.5	0.6	0.9

6. RESULTS

6.1. URANIUM MOLYBDENUM

The swarm evolutions for the thermal, epithermal, and URR uranium optimizations are shown in Figures 6.1-6.9. Generation 1 shows the swarms initial positions with random velocity vectors as black arrows. Each particle is assigned a color: if k_{eff} is above 1.01 it is red, if below 0.99 blue, and if in between it is green (near critical). All of the positions in between the particles on the search space are given a color based on their k_{eff} by linearly interpolating data in between the particles. As the swarm evolves, this contour data is continuously re-interpolated as more positions on the search space are evaluated.

Similarly, the sensitivity plots show the evolution of the swarm and plots each particle's color depending on their k_{eff}. The contour of the sensitivity plot is the energy integrated sensitivity calculated by MCNP at that location. Once again, data is linearly interpolated for positions in between particles on the search space and is updated each generation.

Markers are kept where ever a particle has been in a previous generation, while particle's locations from the most recent generation are shown with their velocity vectors.

A summary of optimized dimensions, sensitives, convergence performance, and improvement when compared to the conventional parameter sweep method can be seen in Table 6.1. The total number of possible configurations in the search space is 10,000. The improvement metric represents factor of decrease between 10,000 and the total number of configurations the algorithm evaluated before converging.

6.1.1. Thermal. The thermal swarm evolution can be seen in Figure 6.2. Upon completion of the 15th generation, the convergence criteria defined in Section 4.5 was met as seen in Figure 6.1. The swarm converged at a point on the critical line where the thermal sensitivity was highest as shown in Figure 6.2. From the interpolated k_{eff} data it can be

Table 6.1. Uranium Optimization Results

Energy Range	d_1[cm] Polyethylene	d_2[cm] Molybdenum	k_{eff} $\pm[pcm]$	$S_{\text{eff},\sigma}$ ^{95}Mo(n,γ)	Generations	Total Inputs	Improvement
Thermal	3.30	1.25	1.00870±40	-0.0341±0.001	15	225	44.45x
Epithermal	1.05	2.55	1.00199±36	-0.0713±0.0009	12	180	55.56x
URR	0.30	1.50	0.99907±28	-0.0382±0.0003	30	450	15x

seen that initially as the polyethylene plate thickness increases, molybdenum plate thickness must also be increased in order to keep the system critical. In this region the system is under-moderated. Past a polyethylene plate thickness of around 1.5 cm, this trend reverses and molybdenum plate thickness must be decreased in order to keep the system critical. In this region the system is over-moderated.

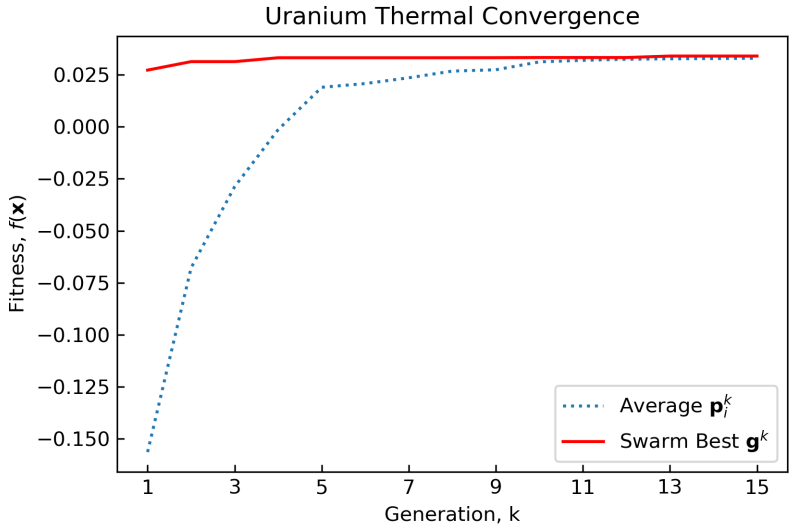

Figure 6.1. Uranium Thermal Convergence

When additional polyethylene is added to an over-moderated system the average neutron energy decreases more and more. This puts more neutrons in our energy region of interest. However, since molybdenum must be removed to maintain criticality the sensitivity to the ^{95}Mo capture cross section will eventually begin to decrease. This can been seen in the interpolated sensitivity plots in Figure 6.3.

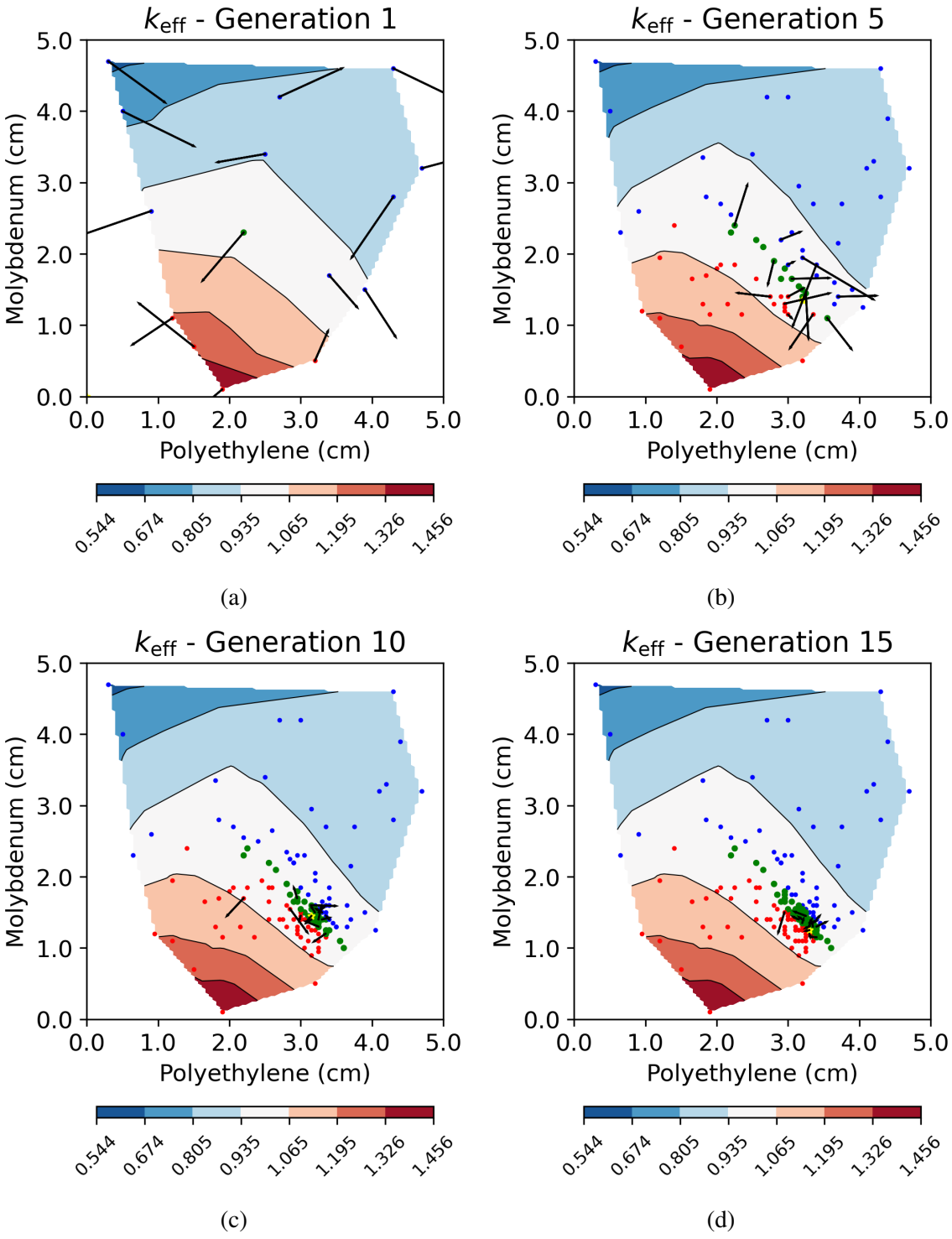

Figure 6.2. Uranium Molybdenum Thermal k_{eff}

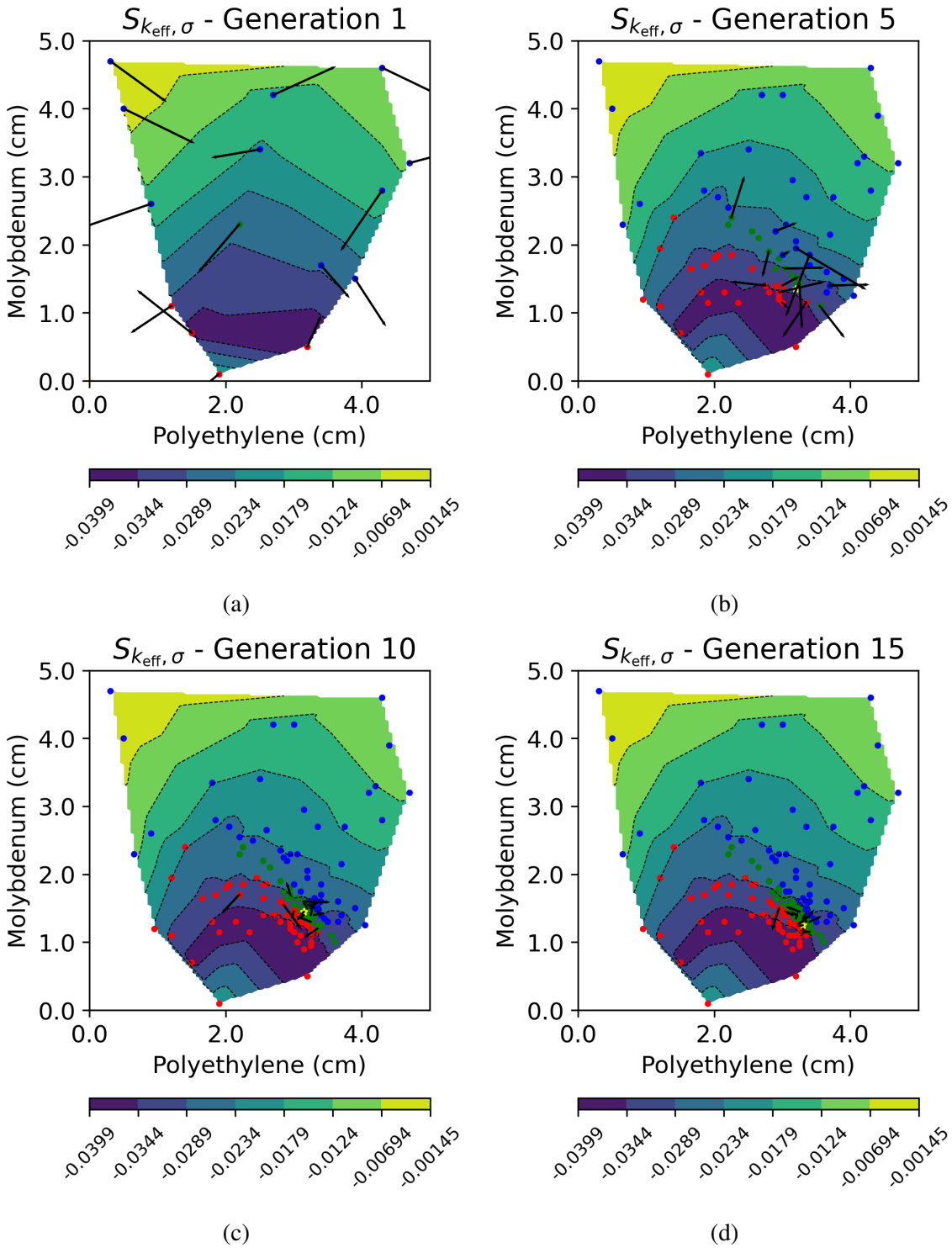

Figure 6.3. Uranium Molybdenum Thermal Sensitivity

6.1.2. Epithermal. The epithermal swarm evolution can be seen in Figures 6.5 and 6.6. Upon completion of the 12th generation, the convergence criteria was met as seen in Figure 6.4. Since this swarm is populated on an identical search space as the thermal optimization the, same critical line was identified. The location on this critical line that the swarm converges was be different our energy range is interest is now higher than previous (0.625 eV - 2 keV), therefore a system with a harder spectrum becomes necessary. The swarm converges at a location on the critical line with less polyethylene than the previous optimization.

The convergence point was on the left half of the critical line, where the system is under-moderated. In this region, the addition of polyethylene must be countered by the addition of molybdenum to keep the system from becoming supercritical. As seen in Figures 6.5 and 6.6, the initial particle locations did not sample the upper left corner of the search space very well. If the optimal point was located in that region, the swarm would likely take longer to converge. To prevent this, more particles could be sampled.

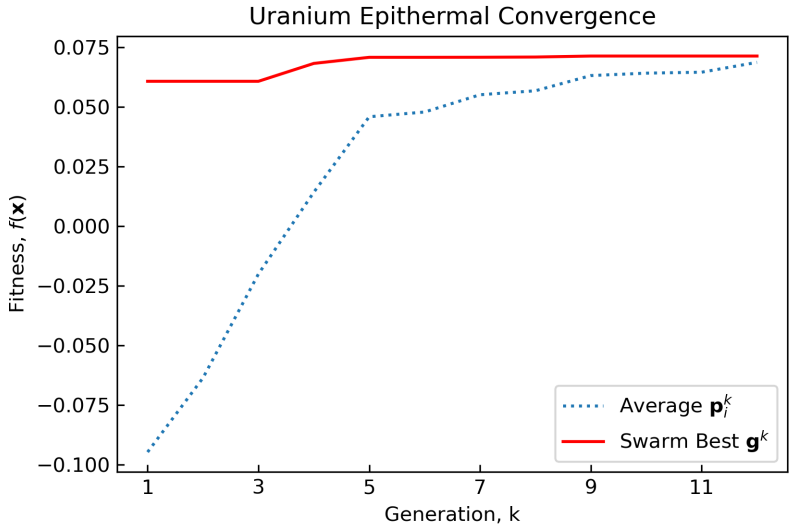

Figure 6.4. Uranium Epithermal Convergence

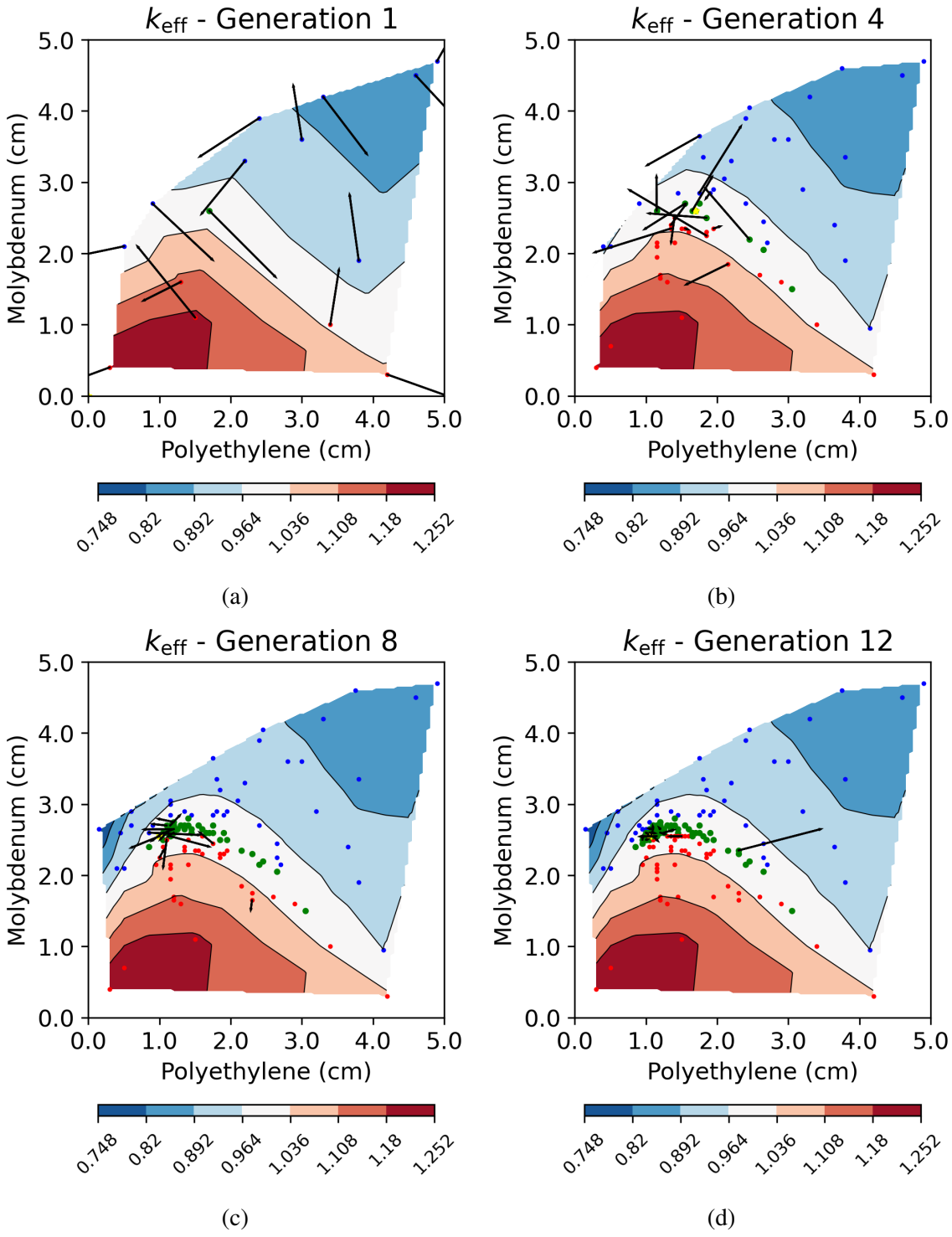

Figure 6.5. Uranium Molybdenum Epithermal k_{eff}

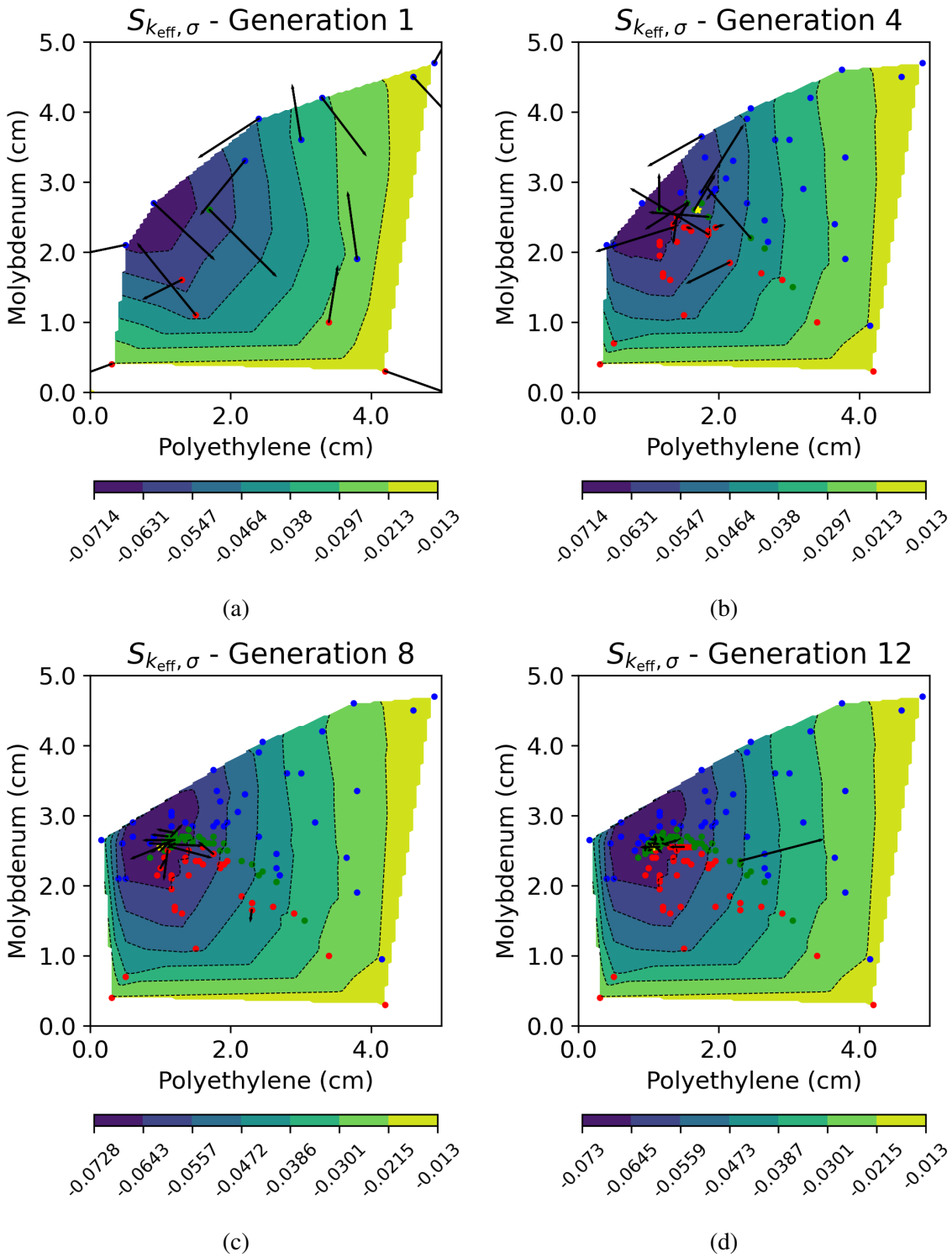

Figure 6.6. Uranium Molybdenum Epithermal Sensitivity

6.1.3. Unresolved Resonance Region. The URR swarm evolution can be seen in Figures 6.8 and 6.9. Compared to the previous two optimizations, this swarm took about twice as many generations in order to converge as seen in Figure 6.7. This can be at least partially attributed to the fact the optima the swarm converged on was located on the edge of the search space where no particles were initially sampled. Due to the poor sampling in this area, the swarm took longer to converge. To combat this, more particles could be sampled.

The position the swarm did converge on was further to the left on the critical line than the thermal and epithermal cases. This is as expected since the less polyethylene, the harder the neutron spectrum. For this high energy case, a higher sensitivity may be achieved using a different moderator. By atom fraction, polyethylene is two-thirds hydrogen. With an atomic mass of just one, neutrons scatting off the hydrogen can be thermalized out of our energy range of interest (2 -200 keV) in only a few scatters.

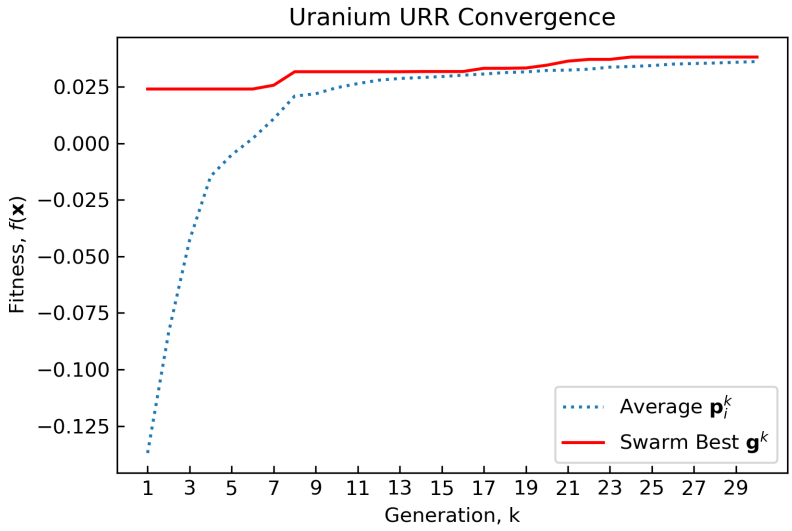

Figure 6.7. Uranium URR Convergence

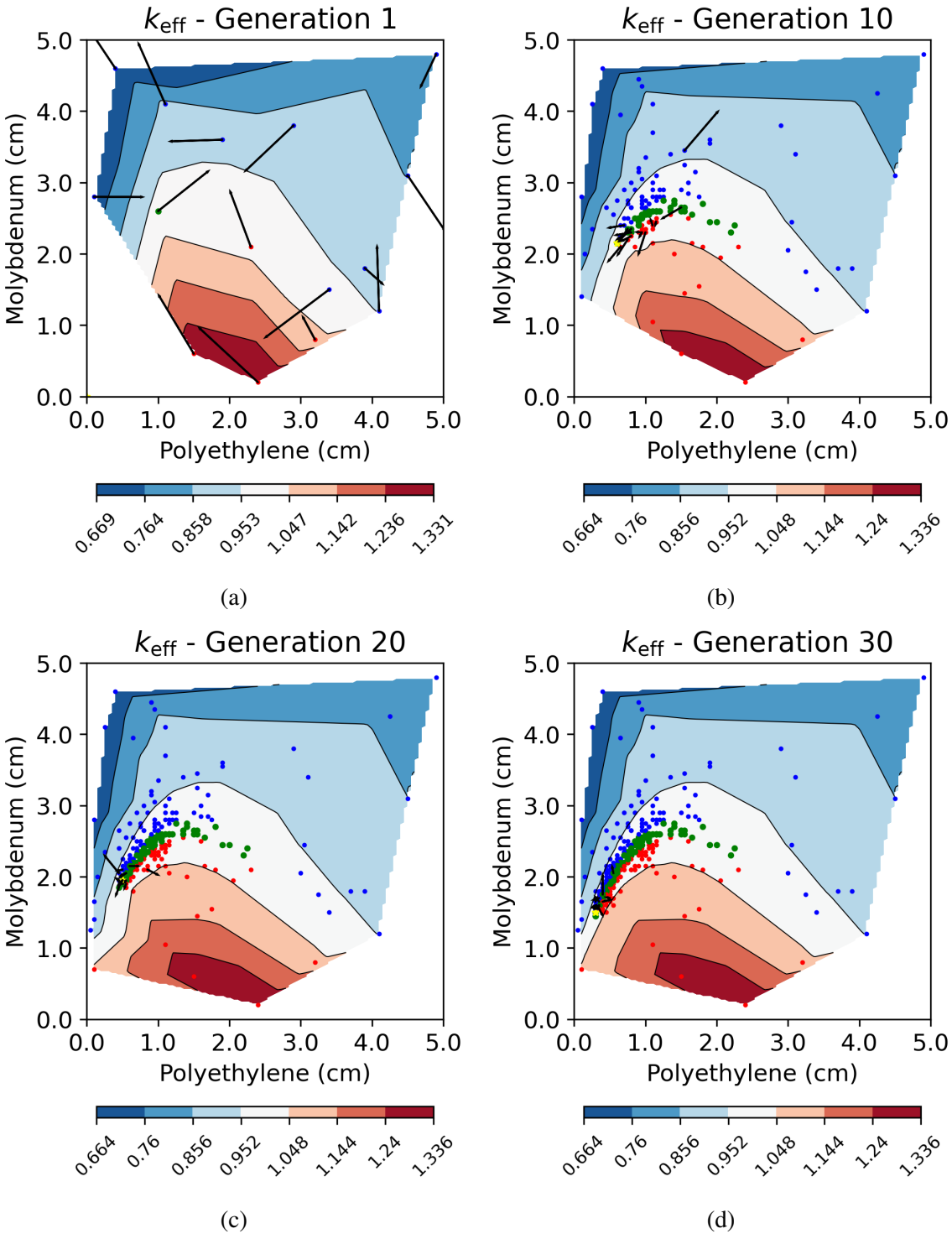

Figure 6.8. Uranium Molybdenum URR k_{eff}

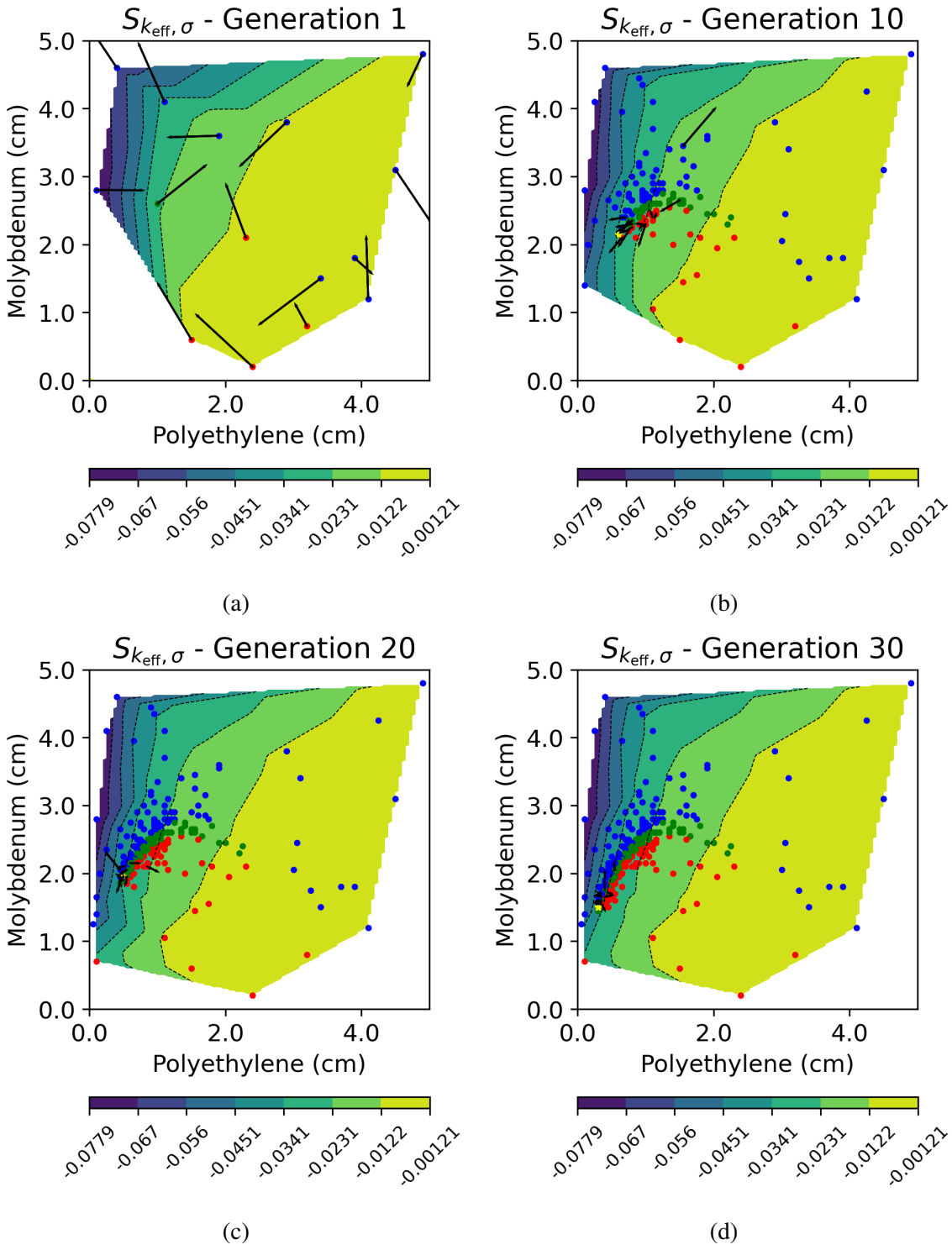

Figure 6.9. Uranium Molybdenum URR Sensitivity

6.2. PLUTONIUM MOLYBDENUM

The swarm evolutions for the thermal, epithermal, and URR plutonium optimizations are shown in Figures 6.10, 6.13, and 6.16. Each dot represents a location a particle has been. Each dot is once again assigned a color: if k_{eff} is above 1.01 it is red, if below 0.99 blue, and if in between it is green (near critical).

From this k_{eff} data a critical surface is interpolated for each optimization seen in Figures 6.11, 6.14, and 6.17. Each point on this surface represents a location on the search space where a critical system exists according to this interpolation. The color on the surface represents the sensitivity to the ^{95}Mo capture cross section for the given energy range.

A summary of optimized dimensions, sensitives, convergence performance, and percentage improvement when compared to the conventional parameter sweep method can be seen in Table 6.2. The total number of possible configurations in the search space is 4,000,000. The improvement metric represents factor of decrease between 4,000,000 and the total number of configurations the algorithm evaluated before converging.

Table 6.2. Plutonium Optimization Results

Energy Range	d_1[cm] Polyethylene	d_2[cm] Molybdenum	d_3[cm] Reflector	k_{eff} $\pm[pcm]$	$S_{k_{\text{eff}},\sigma}$ ^{95}Mo(n,γ)	Generations	Total Inputs	Improvement
Thermal	3.75	1.40	20.00	0.99412±22	-0.0673±0.0006	49	1,225	3265x
Epithermal	1.80	1.55	13.45	1.00954±25	-0.0573±0.0005	42	1,050	3810x
URR	0.85	1.15	10.35	0.99517±25	-0.0130±0.0011	58	1,450	2758x

6.2.1. Thermal. The thermal swarm converged upon the completion of the 49th generation as seen in Figure 6.12. When only looking at the polyethylene and molybdenum dimensions, we see a familiar relationship in Figure 6.10. Initially, as the polyethylene thickness increases, more molybdenum can be accommodated and at a certain point when the system becomes over-moderated the opposite becomes true. Similarly to the uranium thermal optimization, the swarm converged on a configuration that is over-moderated. The swarm converged on a location with a reflector thickness of 20.0 cm, the maximum

value for the search space. The thicker the reflector, the fewer neutrons are leaked and the more molybdenum can be accommodated. This relationship can be seen in Figure 6.11, as reflector thickness increases more and more molybdenum can be introduced while maintaining criticality. Since the energy range of interest for this sensitivity optimization is 0 - 0.625 eV, even very thermal neutrons will contribute to this sensitivity. As we will see in the following optimizations, this trend does not hold true for higher energy ranges of interest.

6.2.2. Epithermal. The epithermal swarm converged upon the completion of the 42nd generation as seen in Figure 6.15. Similarly to the uranium epithermal optimization, the swarm converged on a slightly under-moderated. Unlike the previous optimization the reflector thickness was found to be 13.45 cm. Although the system can accommodate more molybdenum as the reflector thickness increases, the average neutron energy decreases. This contributes to less sensitivity to our energy range of 0.625 eV to 2 keV. This causes the swarm to seek a reflector thickness that allows the most molybdenum without causing too much softening the energy spectrum.

6.2.3. Unresolved Resonance Region. The URR swarm converged upon the completion of the 58th generation as seen in Figure 6.18. As expected, the swarm converged on an under-moderated location on the critical surface and with a reflector thickness of 10.35 cm. As our energy range of interest (2 keV - 200 keV) is higher than the previous, the polyethylene plate and reflector thicknesses decrease. The algorithm must perform a balancing act when identifying a reflector thickness. Too thick and the returning neutrons will be thermalized past our energy range of interest, too thin and less molybdenum can be accommodate by the system, decreasing the sensitivity.

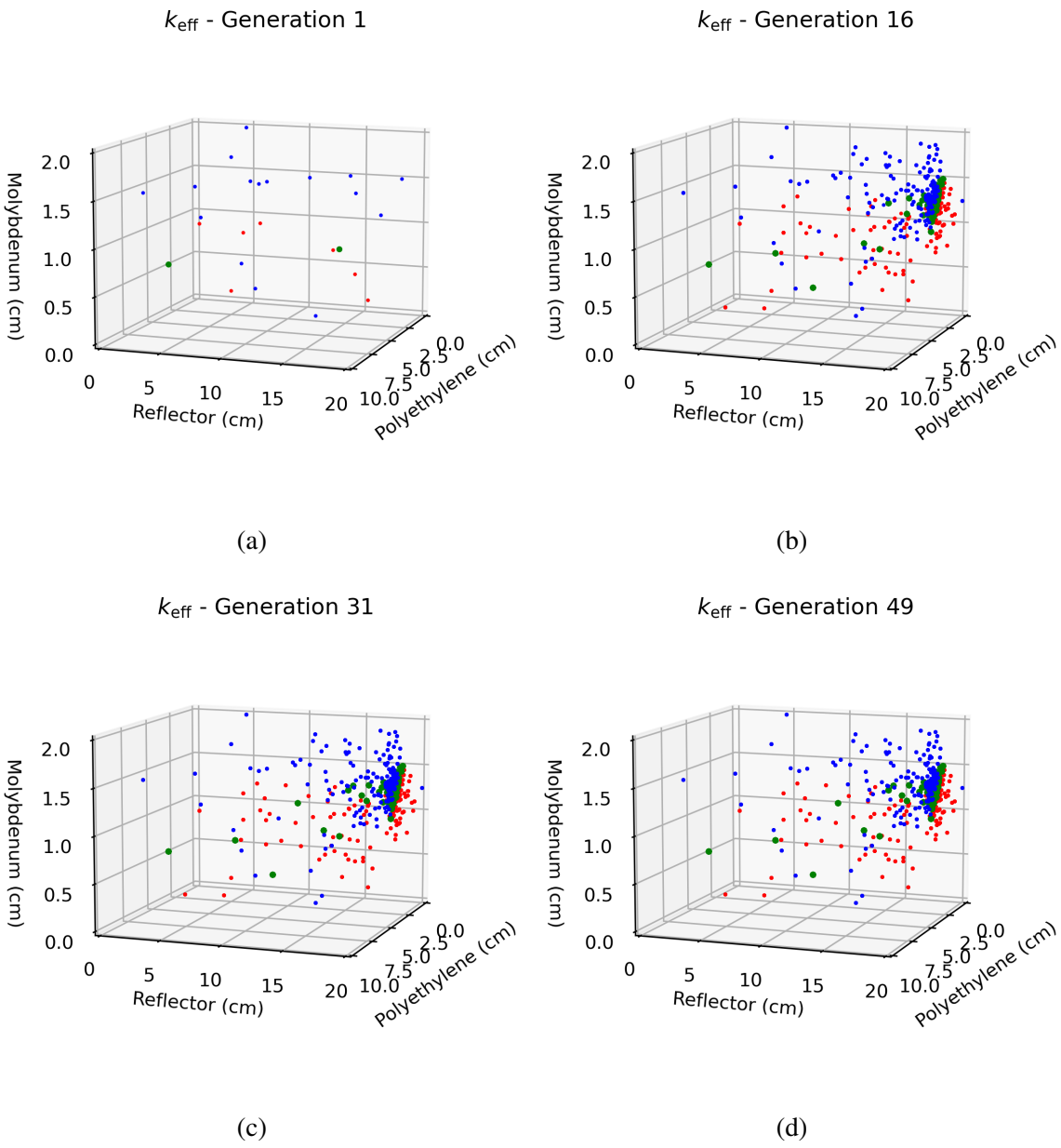

Figure 6.10. Plutonium Molybdenum Thermal k_{eff}

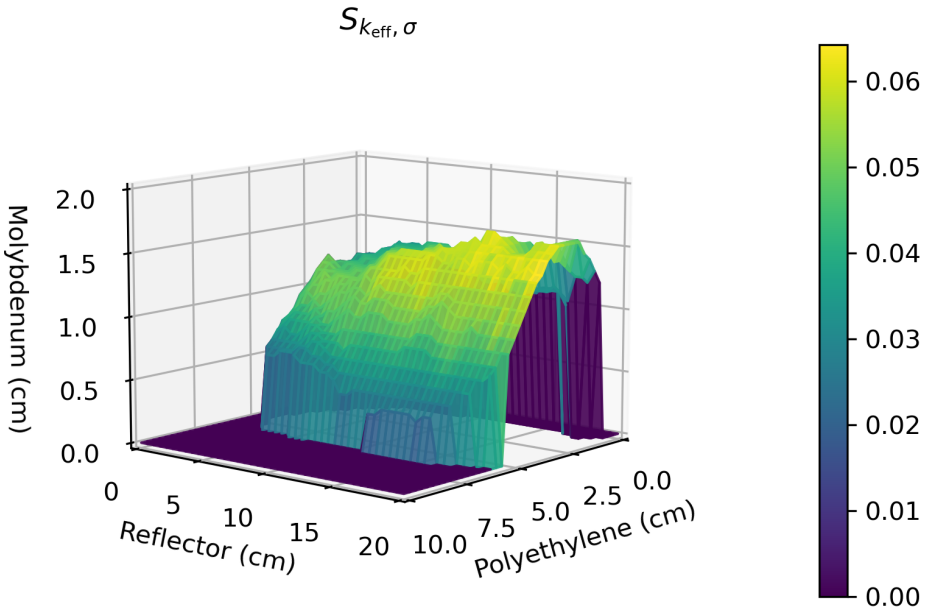

Figure 6.11. Plutonium Thermal Sensitivity

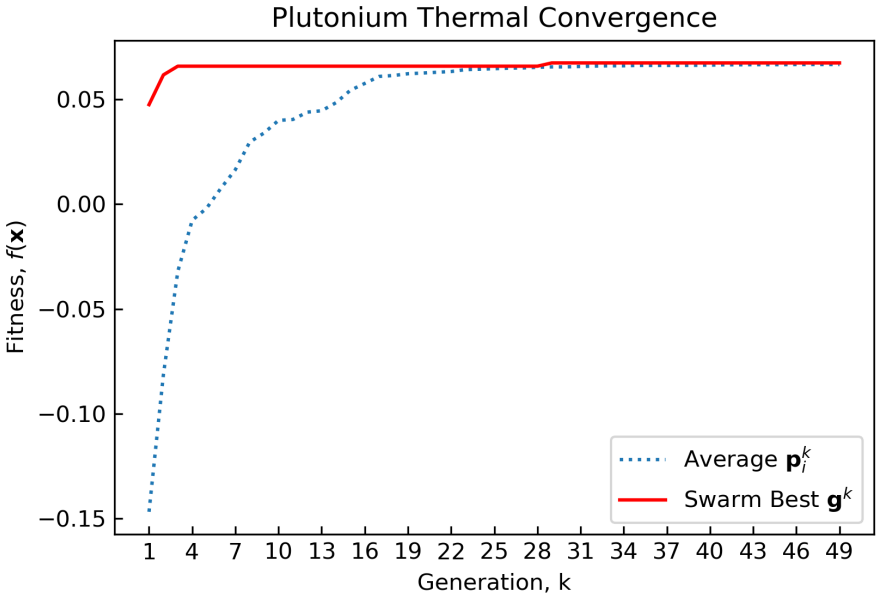

Figure 6.12. Plutonium Thermal Convergence

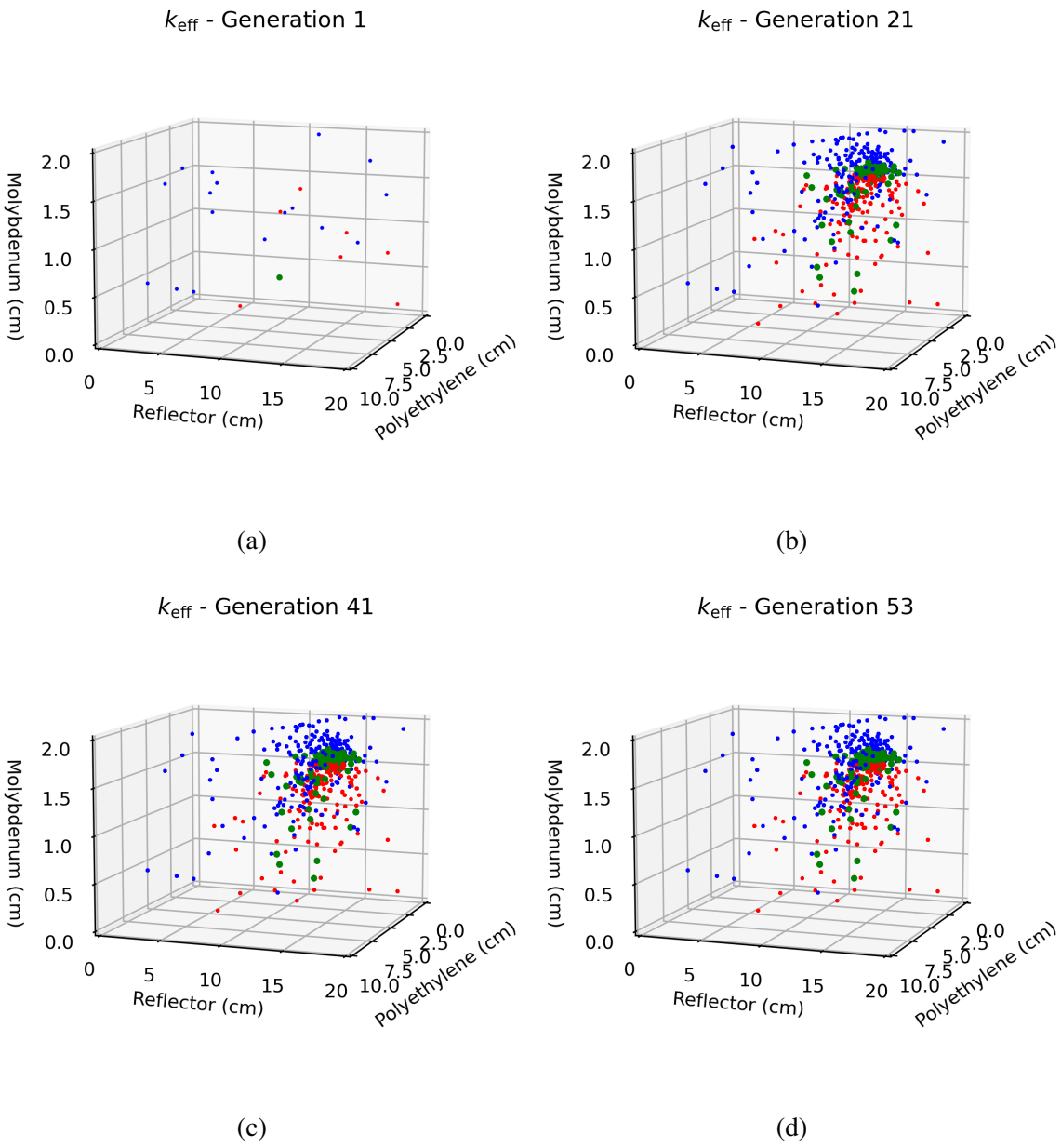

Figure 6.13. Plutonium Molybdenum Epithermal k_{eff}

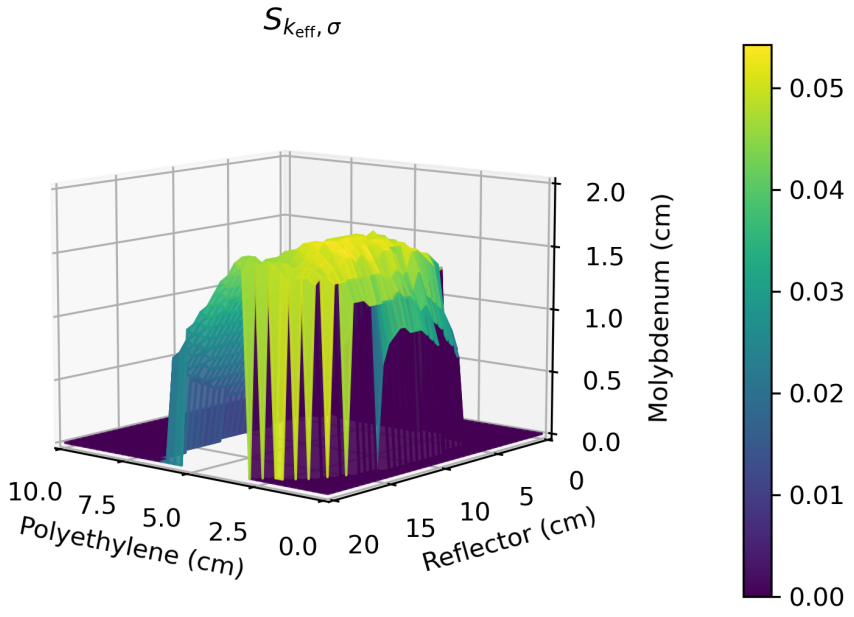

Figure 6.14. Plutonium Epithermal Sensitivity

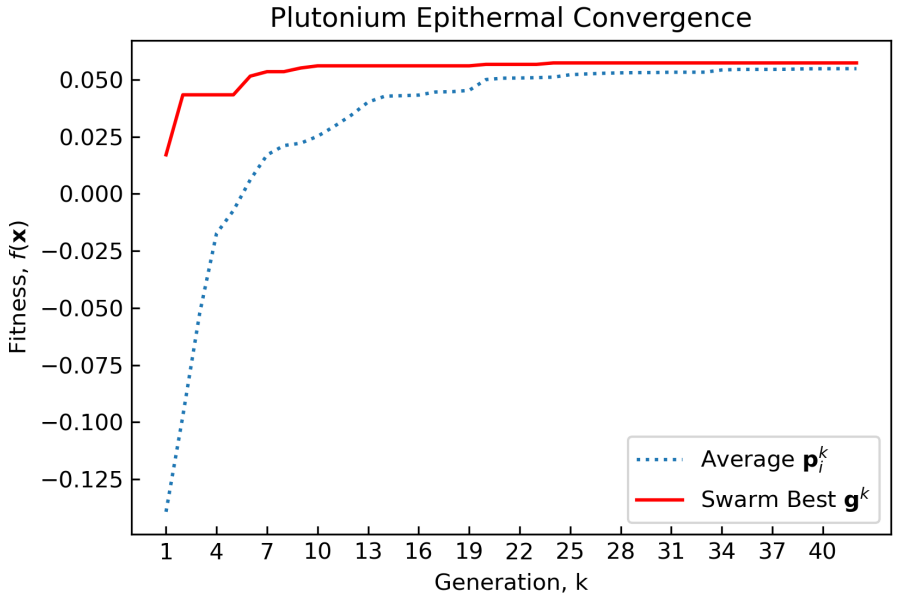

Figure 6.15. Plutonium Epithermal Convergence

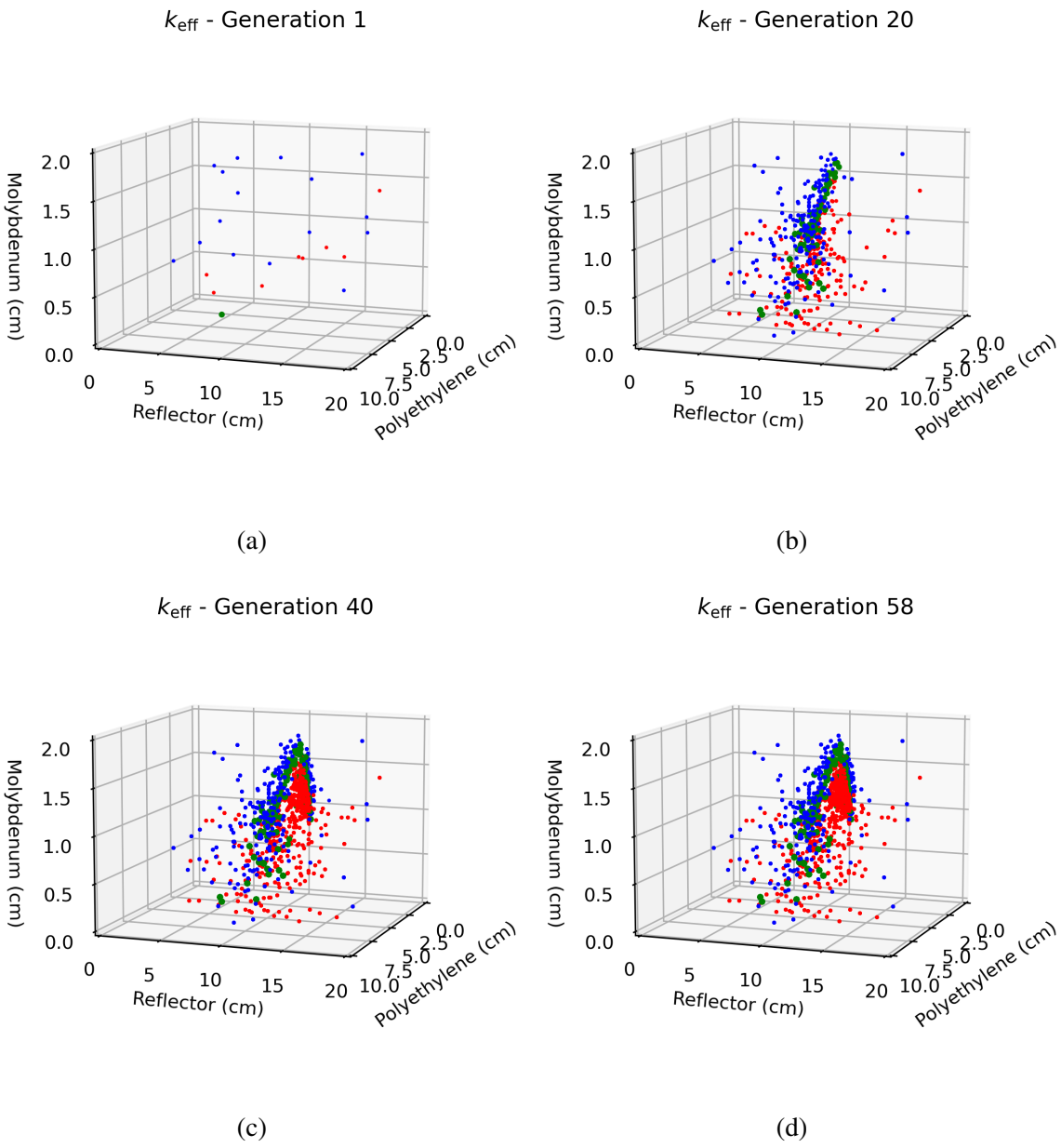

Figure 6.16. Plutonium Molybdenum URR k_{eff}

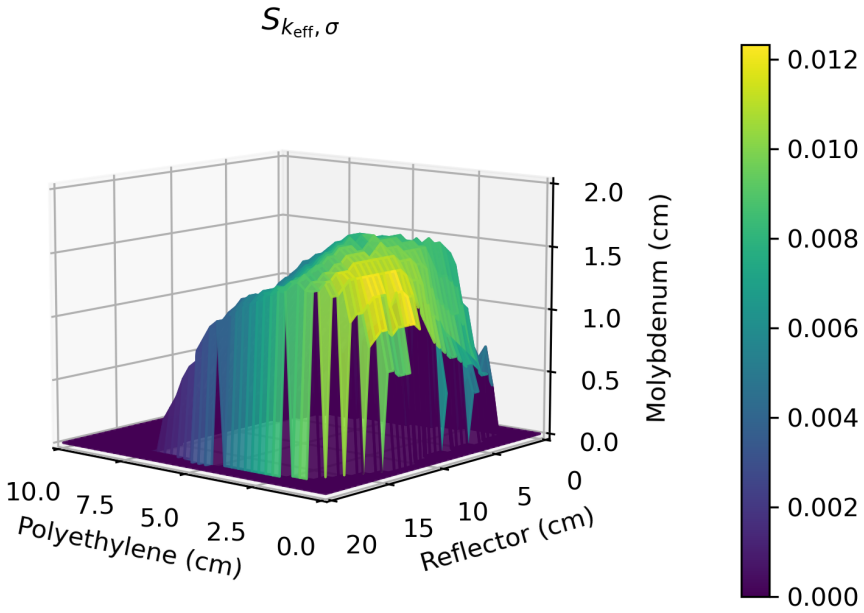

Figure 6.17. Plutonium URR Sensitivity

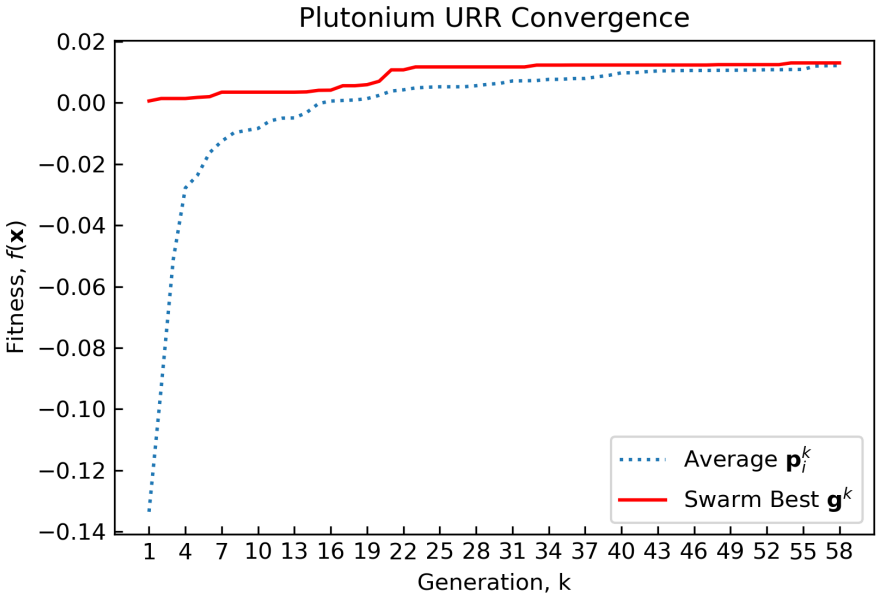

Figure 6.18. Plutonium URR Convergence

7. CONCLUSIONS

A new method of identifying optimal critical configurations was presented. This method used a PSO-MCNP coupled algorithm and was demonstrated on a series of two and three-dimensional molybdenum critical experiments. On average the algorithm performed 35x faster for a two-dimensional and 3277x faster for a three-dimensional optimization than the traditional parameter sweep method. Each simulation took on average 50 seconds to evaluate, this corresponds to 5.6 days and 2,314 days in computational time saved respectively. Since the total number of configurations increases exponentially as more dimensions are added, this algorithm will perform more and more efficiently compared to the parameter sweep method as problems get more complex.

Unlike the optimizations performed in this work, the search space may not always be free of local optima. In cases where there are, additional tuning of the inertial, cognitive, and social weights will become necessary to prevent premature convergence to one of these local optima.

Future efforts on this project may include implementing "adaptive" parameter weight selection [40]. This would allow the algorithm to automatically determine the most optimal parameter weights as the swarm evolves, allowing for more efficient swarm convergence.

APPENDIX A.

URANIUM REFERENCE GEOMETRY MCNP6.2 INPUT

```
TWO-DIMENSIONAL URANIUM REFERENCE GEOMETRY                    1
c d_1 = 0.1 cm                                                2
c d_2 = 0.1 cm                                                3
c                                                             4
c ===============================================           5
C CELL CARDS                                                  6
c ===============================================           7
c                                                             8
c UNIT 1 of 12                                                9
20 3 -10.2 -11 195 -196 imp:n=1 $ Molybdenum                  10
21 2 -0.93 -11 196 -197 imp:n=1 $ Polyethylene                11
22 1 -18.7 -11 197 -198 imp:n=1 $ Jemima                      12
23 2 -0.93 -11 198 -199 imp:n=1 $ Polyethylene                13
24 3 -10.2 -11 199 -200 imp:n=1 $ Molybdenum                  14
c                                                             15
c UNIT 2 of 12                                                16
25 3 -10.2 -11 200 -201 imp:n=1 $ Molybdenum                  17
26 2 -0.93 -11 201 -202 imp:n=1 $ Polyethylene                18
27 1 -18.7 -11 202 -203 imp:n=1 $ Jemima                      19
28 2 -0.93 -11 203 -204 imp:n=1 $ Polyethylene                20
29 3 -10.2 -11 204 -205 imp:n=1 $ Molybdenum                  21
c                                                             22
c UNIT 3 of 12                                                23
30 3 -10.2 -11 205 -206 imp:n=1 $ Molybdenum                  24
31 2 -0.93 -11 206 -207 imp:n=1 $ Polyethylene                25
32 1 -18.7 -11 207 -208 imp:n=1 $ Jemima                      26
```

```
33 2 -0.93 -11 208 -209 imp:n=1 $ Polyethylene
34 3 -10.2 -11 209 -210 imp:n=1 $ Molybdenum
c
c UNIT 4 of 12
35 3 -10.2 -11 210 -211 imp:n=1 $ Molybdenum
36 2 -0.93 -11 211 -212 imp:n=1 $ Polyethylene
37 1 -18.7 -11 212 -213 imp:n=1 $ Jemima
38 2 -0.93 -11 213 -214 imp:n=1 $ Polyethylene
39 3 -10.2 -11 214 -215 imp:n=1 $ Molybdenum
c
c UNIT 5 of 12
40 3 -10.2 -11 215 -216 imp:n=1 $ Molybdenum
41 2 -0.93 -11 216 -217 imp:n=1 $ Polyethylene
42 1 -18.7 -11 217 -218 imp:n=1 $ Jemima
43 2 -0.93 -11 218 -219 imp:n=1 $ Polyethylene
44 3 -10.2 -11 219 -220 imp:n=1 $ Molybdenum
c
c UNIT 6 of 12
45 3 -10.2 -11 220 -221 imp:n=1 $ Molybdenum
46 2 -0.93 -11 221 -222 imp:n=1 $ Polyethylene
47 1 -18.7 -11 222 -223 imp:n=1 $ Jemima
48 2 -0.93 -11 223 -224 imp:n=1 $ Polyethylene
49 3 -10.2 -11 224 -225 imp:n=1 $ Molybdenum
c
c UNIT 7 of 12
50 3 -10.2 -11 225 -226 imp:n=1 $ Molybdenum
51 2 -0.93 -11 226 -227 imp:n=1 $ Polyethylene
```

```
52 1 -18.7 -11 227 -228 imp:n=1 $ Jemima
53 2 -0.93 -11 228 -229 imp:n=1 $ Polyethylene
54 3 -10.2 -11 229 -230 imp:n=1 $ Molybdenum
c
c UNIT 8 of 12
55 3 -10.2 -11 230 -231 imp:n=1 $ Molybdenum
56 2 -0.93 -11 231 -232 imp:n=1 $ Polyethylene
57 1 -18.7 -11 232 -233 imp:n=1 $ Jemima
58 2 -0.93 -11 233 -234 imp:n=1 $ Polyethylene
59 3 -10.2 -11 234 -235 imp:n=1 $ Molybdenum
c
c UNIT 9 of 12
60 3 -10.2 -11 235 -236 imp:n=1 $ Molybdenum
61 2 -0.93 -11 236 -237 imp:n=1 $ Polyethylene
62 1 -18.7 -11 237 -238 imp:n=1 $ Jemima
63 2 -0.93 -11 238 -239 imp:n=1 $ Polyethylene
64 3 -10.2 -11 239 -240 imp:n=1 $ Molybdenum
c
c UNIT 10 of 12
65 3 -10.2 -11 240 -241 imp:n=1 $ Molybdenum
66 2 -0.93 -11 241 -242 imp:n=1 $ Polyethylene
67 1 -18.7 -11 242 -243 imp:n=1 $ Jemima
68 2 -0.93 -11 243 -244 imp:n=1 $ Polyethylene
69 3 -10.2 -11 244 -245 imp:n=1 $ Molybdenum
c
c UNIT 11 of 12
70 3 -10.2 -11 245 -246 imp:n=1 $ Molybdenum
```

```
71 2 -0.93 -11 246 -247 imp:n=1 $ Polyethylene
72 1 -18.7 -11 247 -248 imp:n=1 $ Jemima
73 2 -0.93 -11 248 -249 imp:n=1 $ Polyethylene
74 3 -10.2 -11 249 -250 imp:n=1 $ Molybdenum
c
c UNIT 12 of 12
75 3 -10.2 -11 250 -251 imp:n=1 $ Molybdenum
76 2 -0.93 -11 251 -252 imp:n=1 $ Polyethylene
77 1 -18.7 -11 252 -253 imp:n=1 $ Jemima
78 2 -0.93 -11 253 -254 imp:n=1 $ Polyethylene
79 3 -10.2 -11 254 -255 imp:n=1 $ Molybdenum
c
1000 4 -8.96   -300  (11:255:-195) imp:n=1 $reflector
1001 0          300                imp:n=0 $graveyard
c EOCC

c ================================================
C SURF CARDS
c ================================================
c UNIT 1 of 12
195 pz -5
196 pz -4.9
197 pz -4.8
198 pz -4.5
199 pz -4.4
c
c UNIT 2 of 12
```

```
200 pz -4.3                                                    108
201 pz -4.2                                                    109
202 pz -4.1                                                    110
203 pz -3.8                                                    111
204 pz -3.7                                                    112
c                                                              113
c UNIT 3 of 12                                                 114
205 pz -3.6                                                    115
206 pz -3.5                                                    116
207 pz -3.4                                                    117
208 pz -3.1                                                    118
209 pz -3.0                                                    119
c                                                              120
c UNIT 4 of 12                                                 121
210 pz -2.9                                                    122
211 pz -2.8                                                    123
212 pz -2.7                                                    124
213 pz -2.4                                                    125
214 pz -2.3                                                    126
c                                                              127
c UNIT 5 of 12                                                 128
215 pz -2.2                                                    129
216 pz -2.1                                                    130
217 pz -2.0                                                    131
218 pz -1.7                                                    132
219 pz -1.6                                                    133
c                                                              134
```

```
c UNIT 6 of 12
220 pz -1.5
221 pz -1.4
222 pz -1.3
223 pz -1.0
224 pz -0.9
c
c UNIT 7 of 12
225 pz -0.8
226 pz -0.7
227 pz -0.6
228 pz -0.3
229 pz -0.2
c
c UNIT 8 of 12
230 pz -0.1
231 pz -0.0
232 pz 0.1
233 pz 0.4
234 pz 0.5
c
c UNIT 9 of 12
235 pz 0.6
236 pz 0.7
237 pz 0.8
238 pz 1.1
239 pz 1.2
```

```
c                                                                    162
c UNIT 10 of 12                                                      163
240 pz 1.3                                                           164
241 pz 1.4                                                           165
242 pz 1.5                                                           166
243 pz 1.8                                                           167
244 pz 1.9                                                           168
c                                                                    169
c UNIT 11 of 12                                                      170
245 pz 2.0                                                           171
246 pz 2.1                                                           172
247 pz 2.2                                                           173
248 pz 2.5                                                           174
249 pz 2.6                                                           175
c                                                                    176
c UNIT 12 of 12                                                      177
250 pz 2.7                                                           178
251 pz 2.8                                                           179
252 pz 2.9                                                           180
253 pz 3.2                                                           181
254 pz 3.3                                                           182
c                                                                    183
c extra surfaces                                                     184
10  so  200                                                          185
11  cz  26.67                                                        186
13  pz -19.42                                                        187
255 pz 3.4                                                           188
```

```
256 pz 17.82                                                    189
300 BOX -44.1452 -44.1452 -20                                   190
         88.29     0        0                                   191
          0        88.29    0                                   192
          0         0       37.82                               193
c                                                               194
c EOSC                                                          195
                                                                196
c ================================================              197
c DATA CARDS                                                    198
c ================================================              199
c                                                               200
KCODE 10000 1.0 30 530                                          201
KSRC 0 0 -4.001                                                 202
     0 0 -3.001                                                 203
     0 0 -2.001                                                 204
     0 0  0.001                                                 205
c ================================================              206
c Materials                                                     207
c ------------------------------------------------              208
C HEU, rho=18.7g/cc                                             209
c ------------------------------------------------              210
M1  92235.80c 0.93 92238.80c 0.07                               211
c                                                               212
c ------------------------------------------------              213
C Moderator                                                     214
c ------------------------------------------------              215
```

```
c Polyethylene, rho=0.93g/cc                                    216
M2  6000.80c -0.856284 1001.80c -0.14371                        217
MT2 h-poly.80t                                                  218
c                                                               219
c ------------------------------------------------              220
C Interstitial                                                  221
c ------------------------------------------------              222
C Molybdenum, rho=10.22g/cc                                     223
M3  42092.80c 0.1465 42094.80c 0.0919                           224
    42095.80c 0.1587 42096.80c 0.1667                           225
    42097.80c 0.0958 42098.80c 0.2429                           226
    42100.80c 0.0974                                            227
c                                                               228
c ------------------------------------------------              229
C Reflector                                                     230
c ------------------------------------------------              231
c Copper, rho=8.96g/cc                                          232
M4  29063.80c 5.7213E-02                                        233
    29065.80c 2.5501E-02                                        234
c                                                               235
c Material cards from:                                          236
c "Compendium of Material Composition Data                      237
c for Radiation Transport Modeling"-PNNL                        238
c                                                               239
KSEN2 XS ISO=42095.80c MT=102 ERG = 0.002 0.2                   240
```

APPENDIX B.

PLUTONIUM REFERENCE GEOMETRY MCNP6.2 INPUT

```
THREE-DIMENSIONAL PLUTONIUM REFERENCE GEOMETRY                    1
c d_1 = 0.1 cm                                                    2
c d_2 = 1.0 cm                                                    3
c d_3 = 1.0 cm                                                    4
c ================================================               5
C CELL CARDS                                                      6
c ================================================               7
c Fuel                                                            8
c ------------------------------------------------               9
1 1 -15.1443 &                                                    10
     ( 103 -104 107 -108 105 -106): &                             11
     ( 109 -110 101 -107 105 -106): &                             12
     ( 109 -110 108 -102 105 -106): &                             13
     (-111 110 -107 105 -106): &                                  14
     (-112 108 110 105 -106): &                                   15
     (-113 -109 -107 105 -106): &                                 16
     (-114 108 -109 105 -106) &                                   17
     u=1 imp:n=1                                                  18
c ------------------------------------------------               19
C ZPPR Cladding                                                   20
c ------------------------------------------------               21
2 2 -7.9 &                                                        22
     (201 -204 205 -210 211 -216)                                 23
     (-202:203:-206:209:-212:215) u=1 imp:n=1                     24
4 0 #1 #2 u=1 imp:n=1                                             25
c ------------------------------------------------               26
```

```
C Tray                                                    27
c ------------------------------------------------        28
5 0 201 -204 205 -210 211 -216 u=2 imp:n=1                29
6 0 #5 u=2 imp:n=1                                        30
7 0 201 -204 205 -210 211 -216                            31
    trcl = (2.37963 3.8807065 0)                          32
        lat=1 u=3 imp:n=1                                 33
        fill=-3:4 -2:3 0:0                                34
     2 2 2 2 2 2 2 2                                      35
     2 1 1 1 1 1 1 2                                      36
     2 1 1 1 1 1 1 2                                      37
     2 1 1 1 1 1 1 2                                      38
     2 1 1 1 1 1 1 2                                      39
     2 2 2 2 2 2 2 2                                      40
c                                                         41
701 0 #7 u=3 imp:n=1                                      42
c                                                         43
770 0 -510 u=5 imp:n=1                                    44
780 0 510 u=5 imp:n=1                                     45
c ------------------------------------------------        46
C Molybdenum                                              47
c ------------------------------------------------        48
9 4 -10.22 -510 u=4 imp:n=1                               49
781 0 510 u=4 imp:n=1                                     50
772 0 -510                                                51
        lat=1 u=10 imp:n=1                                52
        fill= -1:4 -6:1 0:0                               53
```

```
     5 5 5 5 5 5                                                    54
     5 4 4 4 4 5                                                    55
     5 4 4 4 4 5                                                    56
     5 4 4 4 4 5                                                    57
     5 4 4 4 4 5                                                    58
     5 4 4 4 4 5                                                    59
     5 4 4 4 4 5                                                    60
     5 5 5 5 5 5                                                    61
c                                                                   62
782 0 #772 u=10 imp:n=1                                             63
873 0 -42 fill=10 u=8 imp:n=1  $Fills Layer with Moly               64
802 0 -1 fill=3 u=8 imp:n=1    $Fills Layer with fuel               65
808 0 #802 #873                                                     66
     u=8 imp:n=1                                                    67
c                                                                   68
c translations for fuel units                                       69
101 0 -40 trcl=(0 0 0.000000) fill=8 imp:n=1                        70
102 0 -40 trcl=(0 0 1.397561) fill=8 imp:n=1                        71
103 0 -40 trcl=(0 0 2.795122) fill=8 imp:n=1                        72
104 0 -40 trcl=(0 0 4.192683) fill=8 imp:n=1                        73
105 0 -40 trcl=(0 0 5.590244) fill=8 imp:n=1                        74
106 0 -40 trcl=(0 0 6.987805) fill=8 imp:n=1                        75
107 0 -40 trcl=(0 0 8.385366) fill=8 imp:n=1                        76
108 0 -40 trcl=(0 0 9.782927) fill=8 imp:n=1                        77
109 0 -40 trcl=(0 0 11.18048) fill=8 imp:n=1                        78
110 0 -40 trcl=(0 0 12.57804) fill=8 imp:n=1                        79
111 0 -40 trcl=(0 0 13.97561) fill=8 imp:n=1                        80
```

```
112 0 -40 trcl=(0 0 15.37317) fill=8 imp:n=1
c
c ---------------------------------------------
C Moderator
c ---------------------------------------------
999 5 -0.93 -99
     #101 #102 #103 #104 #105 #106
     #107 #108 #109 #110 #111 #112
     imp:n=1
c ---------------------------------------------
C Graveyard
c ---------------------------------------------
998 0 99 imp:n=0

c ===============================================
C SURF CARDS
c ===============================================
c ----- Pu, Tray, and Moderator surfaces --------
c
1 rpp -15.31927900 15.31927900
      -15.31927900 15.31927900
       -0.14878050  0.148780500
c
42 rpp -15.31927900
        15.31927900
       -15.31927900
        15.31927900
```

```
         0.148780500                                          108
         1.1487805                                            109
c                                                             110
510 rpp -15.31927900 -7.717059000                             111
         10.251979   15.31927900                             112
         0.148780500  1.1487805                              113
c                                                             114
40 rpp -15.319279000 15.319279000                             115
       -15.319279000 15.319279000                             116
        -0.148780500  1.1487805                              117
c                                                             118
c reflector                                                   119
99 rpp                                                        120
       -16.42 16.42                                           121
       -16.42 16.42                                           122
        -1.15 17.52                                           123
c ------------------------------------------------           124
c Cladding                                                    125
c ------------------------------------------------           126
201 px -2.530729                                              127
202 px -2.287083795                                           128
203 px 2.287083795                                            129
204 px 2.530729                                               130
C ----------------------                                      131
205 py -3.8128575                                             132
206 py -3.7846635                                             133
209 py 3.7846635                                              134
```

```
210 py 3.8128575
C ----------------------
211 pz -0.148780500
212 pz -0.1205865
215 pz 0.1205865
216 pz 0.148780500
c ------------------------------------------------
C Fuel
c ------------------------------------------------
101 1 px -2.21972
102 1 px 2.21972
103 1 py -3.71221
104 1 py 3.71221
105 1 pz -0.10668
106 1 pz 0.10668
c ------------------------------------------------
C Misc Surfs
c ------------------------------------------------
107 1 px -1.58472
108 1 px 1.58472
109 1 py -3.07721
110 1 py 3.07721
111 1 c/z -1.58472 3.07721 0.635
112 1 c/z 1.58472 3.07721 0.635
113 1 c/z -1.58472 -3.07721 0.635
114 1 c/z 1.58472 -3.07721 0.635
```

```
c ================================================          162
c DATA CARDS                                                163
c ================================================          164
mode n                                                      165
kcode 100000 1.0 10 110                                     166
ksrc 1 10 0                                                 167
tr1 0.0 -0.0724535 0.0                                      168
c                                                           169
c ================================================          170
c Materials                                                 171
c ------------------------------------------------          172
C Pu                                                        173
c ------------------------------------------------          174
m1   94239.80c -98.8640 94240.80c  -4.6950                  175
     94241.80c  -0.0276 94242.80c  -0.0050                  176
     95241.80c  -0.4049 92235.80c  -0.1622                  177
     92236.80c  -0.0284 93237.80c  -0.0270                  178
     02004.80c  -0.0037 13027.80c  -1.1584                  179
c                                                           180
c ------------------------------------------------          181
C Cladding                                                  182
c ------------------------------------------------          183
C TYPE 304 SS, rho=8.00g/cc                                 184
m2   6000.80c  -0.000400 4000.60c -0.005000                 185
     15031.80c -0.00023  16000.60c -0.000150                186
     24000.50c -0.190000 25055.80c -0.010000                187
     26000.50c -0.701730 28000.50c -0.092500                188
```

```
c                                                                    189
C Aluminum, rho=2.6989g/cc                                           190
m3 13027.80c -1                                                      191
c                                                                    192
c ------------------------------------------------                   193
C Interstitial                                                       194
c ------------------------------------------------                   195
C Molybdenum, rho=10.22g/cc                                          196
M4   42092.80c 0.1465 42094.80c 0.0919                               197
     42095.80c 0.1587 42096.80c 0.1667                               198
     42097.80c 0.0958 42098.80c 0.2429                               199
     42100.80c 0.0982                                                200
c                                                                    201
c ------------------------------------------------                   202
C Moderator                                                          203
c ------------------------------------------------                   204
c Polyetheylne, rho=0.93g/cc                                         205
M5   1001.80c -0.143716 6000.80c -0.856284                           206
MT5  h-poly.80t                                                      207
c                                                                    208
c Material cards from:                                               209
c "Compendium of Material Composition Data                           210
c for Radiation Transport Modeling"-PNNL                             211
c                                                                    212
c Adapted from IER-532                                               213
c                                                                    214
KSEN2 XS ISO=42095.80c MT=102 ERG = 0.000000625 0.1                  215
```

REFERENCES

[1] H. C. Paxton. Thirty-Five Years at Pajarito Canyon Site. Technical Report LA-7121-H, Los Alamos Scientific Laboratory, 05 1981.

[2] J. Hutchinson et al. Criticality Experiments with Fast 235U and 239Pu Metal and Hydride Systems During the Manhattan Project. *Nuclear Technology*, 207(1):S62–S80, 2021. doi: 10.1080/00295450.2021.1908076.

[3] R. E. Rothe. A Technically Useful History of the Critical Mass Laboratory at Rocky Flats. Technical Report LA-UR-05-3247, Los Alamos National Laboratory, 05 2005.

[4] D. Loaiza and D. Gehman. End of an Era for the Los Alamos Critical Experiments Facility: History of critical assemblies and experiments (1946–2004). *Annals of Nuclear Energy*, 33(17):1339–1359, 2006. ISSN 0306-4549. doi: https://doi.org/10.1016/j.anucene.2006.09.009.

[5] A. Chambers. Special Issue on the National Criticality Experiments Research Center. *Nuclear Science and Engineering*, 195(1):iii–iv, 2021. doi: 10.1080/00295639.2021.1968645.

[6] R. Sanchez et al. A New Era of Nuclear Criticality Experiments: The First 10 Years of Planet Operations at NCERC. *Nuclear Science and Engineering*, 195(1):S1–S16, 2021. doi: 10.1080/00295639.2021.1951077.

[7] N. Thompson et al. A New Era of Nuclear Criticality Experiments: The First 10 Years of Comet Operations at NCERC. *Nuclear Science and Engineering*, 195(1):S17–S36, 2021. doi: 10.1080/00295639.2021.1947105.

[8] D. I. Poston, M. A. Gibson, T. Godfroy, and P. R. McClure. KRUSTY Reactor Design. *Nuclear Technology*, 206(1):S13–S30, 2020. doi: 10.1080/00295450.2020.1725382.

[9] D. Hayes et al. A New Era of Nuclear Criticality Experiments: The First 10 Years of Flattop Operations at NCERC. *Nuclear Science and Engineering*, 195(1):S37–S54, 2021. doi: 10.1080/00295639.2021.1947104.

[10] J. Goda et al. A New Era of Nuclear Criticality Experiments: The First 10 Years of Godiva IV Operations at NCERC. *Nuclear Science and Engineering*, 195(1):S55–S79, 2021. doi: 10.1080/00295639.2021.1947103.

[11] J. Hutchinson et al. A New Era of Nuclear Criticality Experiments: The First 10 Years of Radiation Test Object Operations at NCERC. *Nuclear Science and Engineering*, 195(1):S80–S98, 2021. doi: 10.1080/00295639.2021.1918938.

[12] International Handbook of Evaluated Reactor Physics Benchmark Experiments. *Paris: NEA 7329, OECD Nuclear Energy Agency*, 2017.

[13] M. B. Chadwick D. A. Brown. ENDF/B-VIII.0: The 8th major release of the nuclear reaction data library with CIELO-project cross sections, new standards and thermal scattering data. *Nucl. Data Sheets*, 148, 2018.

[14] A. Saltelli. Sensitivity Analysis for Importance Assessment. *Risk Analysis*, 22(3): 579–590, 2002. doi: 10.1111/0272-4332.00040.

[15] R. Bahran et al. Isotopic molybdenum total neutron cross section in the unresolved resonance region. *Phys. Rev. C*, 92:024601, Aug 2015. doi: 10.1103/PhysRevC.92.024601.

[16] I. Duhamel, N. Leclaire, L. Leal, A. Kimura, and S. Nakamura. Measurement, Evaluations and Validation of Molybdenum Cross Sections. *EPJ Web Conf.*, 247: 09007, 2021. doi: 10.1051/epjconf/202124709007.

[17] N. Thompson, R. Bahran, and J. Hutchinson. Identifying Gaps in Critical Benchmarks.

[18] OECD/NEA Data Bank. The JEFF-3.1.1 Nuclear Data Library. *OECD/NEA Data Bank*, JEFF Report 22, 2009.

[19] O. Iwamoto K. Shibata. JENDL-4.0: A New Library for Nuclear Science and Engineering. *J. Nucl. Sci. Technology*, 48, 2011.

[20] P. Obložinský M .B. Chadwick. ENDF/B-VII.0: Next Generation Evaluated Nuclear Data Library for Nuclear Science and Technology. *Nucl. Data Sheets*, 107, 2006.

[21] S. C. van der Marck. Benchmarking ENDF/B-VII.1, JENDL-4.0 and JEFF-3.1.1 with MCNP6. *Nuclear Data Sheets*, 113(12):2935–3005, 2012. ISSN 0090-3752. doi: https://doi.org/10.1016/j.nds.2012.11.003. Special Issue on Nuclear Reaction Data.

[22] R. Prabhakaran. U-Mo Monolithic Fuel for Nuclear Research and Test Reactors. *JOM*, 69, 12 2017. doi: 10.1007/s11837-017-2612-3.

[23] E. H. Wilson, D. Jaluvka, A. S. Hebden, J. A. Stillman, and L. M. Jamison. U.S. High Performance Research Reactor Preliminary Design Milestone for Conversion to Low Enriched Uranium Fuel.

[24] D. S. Lee. Refractory Metals and Their Industrial Applications. *Materials and Manufacturing Processes*, 5(1):121–123, 1990. doi: 10.1080/10426919008953233.

[25] C. J. Werner. MCNP6.2 Release Notes. Technical Report LA-UR-18-20808, Los Alamos National Laboratory, 2018.

[26] B. C. Kiedrowski and F. B. Brown. Adjoint-Based k-Eigenvalue Sensitivity Coefficients to Nuclear Data Using Continuous-Energy Monte Carlo. *Nuclear Science and Engineering*, 174(3):227–244, 2013. doi: 10.13182/NSE12-46.

[27] B. C. Kiedrowski, F. B. Brown, and P. Wilson. Adjoint-Weighted Tallies for k-Eigenvalue Calculations with Continuous-Energy Monte Carlo. *Nuclear Science and Engineering*, 168(3):226–241, 2011. doi: 10.13182/NSE10-22.

[28] B. C. Kiedrowski. MCNP6.1 k-Eigenvalue Sensitivity Capability: A User's Guide. Technical Report LA-UR-13-22251, Los Alamos National Laboratory, 2013.

[29] R. A. Lefebvre W. A. Wieselquist and Eds. M. A. Jessee. SCALE Code System. Technical Report ORNL/TM-2005/39 Version 6.2.4, Oak Ridge National Laboratory, Oak Ridge, 2020.

[30] J. Kennedy and R. Eberhart. Particle swarm optimization. In *Proceedings of ICNN'95 - International Conference on Neural Networks*, volume 4, pages 1942–1948 vol.4, 1995. doi: 10.1109/ICNN.1995.488968.

[31] H. H. Rosenbrock. An Automatic Method for Finding the Greatest or Least Value of a Function. *The Computer Journal*, 3(3):175–184, 01 1960. ISSN 0010-4620. doi: 10.1093/comjnl/3.3.175.

[32] P Umapathy, V Chinthakunta, and S A Muthukumaraswamy. Particle swarm optimization with various inertia weight variants for optimal power flow solution. *Discrete Dynamics in Nature and Society*, 2010, 01 2010. doi: 10.1155/2010/462145.

[33] L. A. Rastrigin. Extreme Control Systems. *Theoretical Foundations of Engineering Cybernetics Series*, 3, 1974.

[34] G. Van Rossum and F. Drake Jr. *Python Reference Manual*. Centrum voor Wiskunde en Informatica Amsterdam, 1995.

[35] M. D. McKay, R. J. Beckman, and W. J. Conover. Comparison the three methods for selecting values of input variable in the analysis of output from a computer code. doi: 10.1080/00401706.1979.10489755.

[36] D. Hayes and R. Sanchez. Zeus: Fast-Spectrum Critical Assemblies with an Iron – HEU Core Surrounded By A Copper Reflector. *Intl. Handbook of Evaluated Criticality Safety Benchmark Experiments, NEA/NSC/DOC/(95)03/II*, 2006.

[37] R. MOSTELLER and R. BREWER. Intermediate-Spectrum Critical Assemblies with a Graphite-HEU Core Surrounded By A Copper Reflector. *Intl. Handbook of Evaluated Criticality Safety Benchmark Experiments, NEA/NSC/DOC/(95)03/II*, 2004.

[38] H Lawroski, R G Palmer, F W Thalgott, R N Curran, and R G Matlock. Final safety analysis report on the zero power plutonium reactor (zppr) facility. doi: 10.2172/4597664.

[39] M. A. Smith R. M. Lell. ZPR-6 Assembly 10: A Cylindrical Plutonium/Carbon/Stainless Steel Assembly with Stainless Steel and Iron Reflectors. *Intl. Handbook of Evaluated Criticality Safety Benchmark Experiments, NEA/NSC/DOC/(95)03/II*, 1981.

[40] Z. Zhan, J. Zhang, Y. Li, and H. Chung. Adaptive Particle Swarm Optimization. *IEEE Transactions on Systems, Man, and Cybernetics, Part B (Cybernetics)*, 39(6): 1362–1381, 2009. doi: 10.1109/TSMCB.2009.2015956.

VITA

Cole Michael Kostelac was born in Kansas City, Missouri. He received a Bachelors of Science in Nuclear Engineering and a minor in Mathematics with Summa Cum Laude distinction from the Missorui University of Science and Technology in May of 2021. After this, he went on to obtain a Masters of Science in Nuclear Engineering from the same institution in May of 2022.

In August of 2020, Cole received his Senior Reactor Operators licence at the Missouri University of Science and Technology Research Reactor where he is involved in designing and carrying out reactor experiments and trains students to become reactor operators. Since the summer of 2020, he has been a student in the "Advanced Nuclear Technology" group (NEN-2) at Los Alamos National Laboratory.

This work was supported in part by the DOE Nuclear Criticality Safety Program, funded and managed by the National Nuclear Security Administration for the Department of Energy.